Summer 2015: No. 9

gacm Report

the german association for computational mechanics

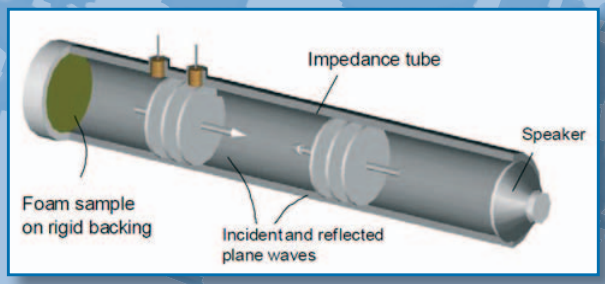

Status on State of Art Simulation with PEM Methods in the Automotive Industry

A. Caillet and D. Blanchet

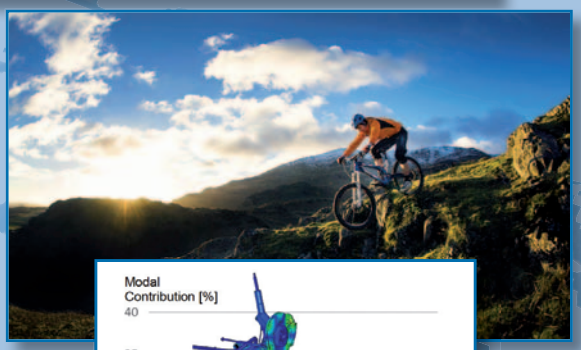

Technology Symbiosis of Topology Optimization and Additive Manufacturing Enables Weight Savings of up to 60 Percent

M. Bromberger

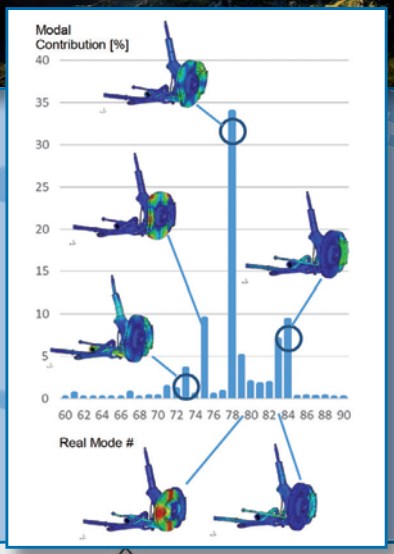

Excellent Brake Noise Comfort by Simulation – Advanced Methods to Create Stability Maps

S. Carvajal Gonzales, D. Wallner, R. Helfrich and M. Klein

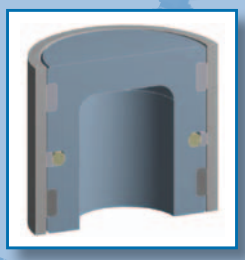

Simulation of Hyperelastic Sealings

C. Gebhardt and N. Nagl

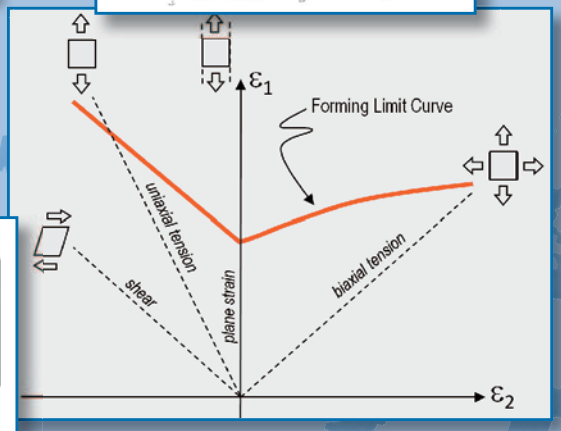

State of the Art in Failure Prediction in Crashworthiness

A. Haufe, F. Andrade
M. Feucht and F. Neukamm

Visit our New Website

Conferences

contents

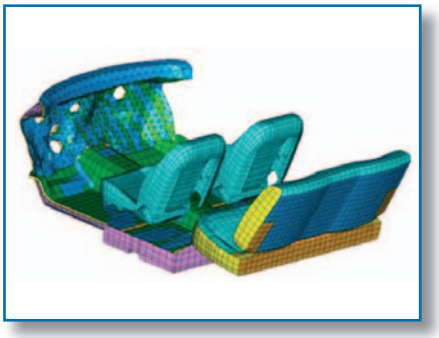

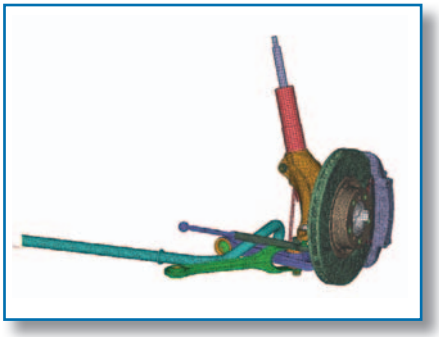

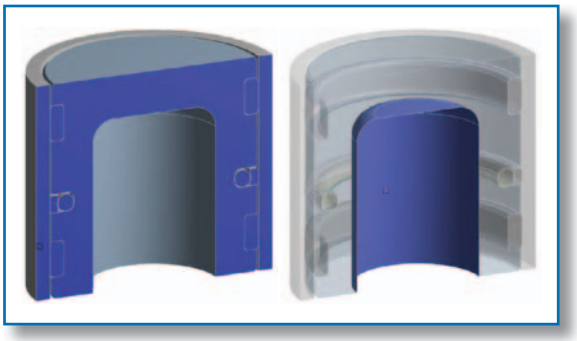

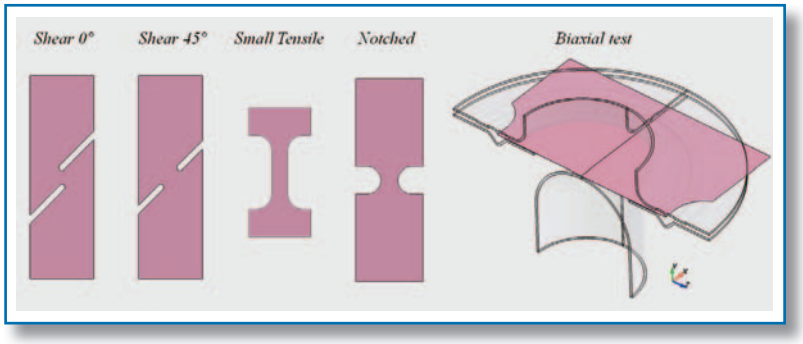

GACM-News

Journal

Conferences

gacmReport

Publisher:
GACM
The German Association for Computational Mechanics

Address:
Institute for Computational Mechanics
Technische Universität München
Boltzmannstrasse 15
D-85747 Garching, Germany
Phone: +49 89 289-15300
Fax: +49 89 289-15301
email: gacm@lnm.mw.tum.de
Internet: www.gacm.de

Editor-in-Chief: Wolfgang A. Wall

Guest Editor: Thomas Münz

Grafik-Design & Print:
K. Schmidle Druck und Medien GmbH, Ebersberg

Print Run: 500

Editorial

Undoubtedly, simulations are indispensable in today's development process of many products. For instance, the development of an automobile without the usage of a variety of simulation tools at all development levels is simply unthinkable these days. This common sense observation is motivation enough to assemble, after some time, another GACM Report which showcases contributions from industry using commercially available Finite Element programs.

Before jumping into this issue of the GACM Report the reader may allow a couple of general remarks and observations on current topics in the commercial environment. Definitely, these comments do not claim any sort of completeness and it is noted that the selected perspective of the observations is biased by the experience in the automotive industry.

Until a couple of years ago, the major, commercially available Finite Element codes used to be associated with specific application fields which they were originally developed for. There were implicit codes for (non-) linear, "slow" dynamic and (quasi-)static applications, explicit programs for crashworthiness studies or other highly dynamic problems, codes for computational fluid dynamics, for acoustics and other specialized fields. This picture has changed considerably in recent years. Basically all major commercial codes are venturing out in neighboring areas and even further, trying to offer solutions for as many application areas as possible. This goal is achieved by either incorporating newly acquired software or by investments in the own development team.

In particular, **multi-physics capabilities** are being developed everywhere. Users are more and more interested in solving simultaneously different physical phenomena which are described by different field equations. The classical example is fluid structure interaction, other examples are the coupling of mechanical and thermal solvers in hot forming processes or the coupling of an electromagnetic with a structural solver. This interaction is achieved either by coupling of two separate codes or by including all the necessary functionality into one code.

At the same time, the maintenance and the development of many specialized in-house programs at universities or inside companies have been stopped or the programs disappeared altogether. Such a development is not very surprising when one considers the cumbersome effort for the continuous maintenance and necessary improvement of these programs. Implementing efficient parallel algorithms or contact algorithms for the sake of solving larger real-world problems can be a big task if the own main focus is on element technology 'only'. As a consequence, it appears desirable that the **commercial programs remain as open as possible** in order to allow researchers to use them for their own developments.

In the past couple of years considerable effort has been directed towards the **development of advanced non-linear material formulations.** Driving forces behind this trend were the extensive material mix used in today's products, the perpetual desire for even more exact simulation results but also the availability of advanced material testing procedures which support the simulation engineer. In the meantime it does not only take an expert for the development of an advanced material formulation but also for the determination of its material parameters.

Process simulations are becoming more and more important in the sense that each simulation is not considered as standalone problem but rather as a sequence of consecutive processes using basically the same or similar model or model parts. The classical example is a crash simulation using the result of a preceding forming simulation. It is important that each step in this process chain is able to interpret and use the outcome of the previous step in an appropriate manner.

An encouraging observation is also, that, finally, **optimization methods** are be-coming more popular in industry. Improved algorithms, better interfaces to the analysis programs and user-friendliness and the availability of less costly hardware lead to the acceptance of these methods. Classical parameter optimization, which is now heavily used for reverse engineering for the determination of material parameters, is accompanied by sensitivity and robustness studies and attempts in using topology optimization algorithms in product development processes.

For all commercial codes **good parallel performance** is of utmost importance. The size and complexity of current models with millions of degrees of freedom is truly remarkable and the success of the simulation codes would not have been possible without the good scalability of the available programs.

This ever increasing need for hardware resources and the pursuit for more flexibility pave directly the way into the cloud. Companies offering **cloud services,** in former times known as "Application Service Providers" put their eyes also on commercial finite element codes. And more and more companies are interested in using these offers for handling peak loads but also for using the facilities on a regular basis. Strangely enough, the discussion about security issues has not dampened these efforts so far.

All the simulations of large models and the consistently increasing number of applications considered lead to the production of a huge amount of data which has to be administered. Furthermore, the work load is shared between teams of engineers all over the world. So-called **Simulation Data Management** tools are being developed to facilitate world-wide collaboration and the handling of data by automating model set-ups, performing quality checks, submitting simulation runs, automating their evaluation and comparing them with experimental results.

Another observation is that the **interaction between industry and academia** could certainly be improved and that better mutual understanding would benefit both sides. There is the impression that academia is not always aware what complex problems are already being tackled and solved in industry and that sometimes rather pragmatic approaches are needed and might work very well. On the other hand, the industrial side is struggling with tracking down the newest developments in academia and has to acknowledge that the development of new methods needs time, money and personnel. Platforms that foster this exchange of ideas, actions and needs are highly appreciated!

Last but not least: the development of commercial codes and their application **need experts in computational mechanics.** It is very positive to see a fair amount of degree programs being established over the last decade and longer as an addition to the still indispensable standard engineering courses. Besides teaching the necessary theoretical background a first hands-on experience with industrial codes might trigger a student's interest to work later in the field of computational mechanics.

The present issue of the GACM Report showcases five papers from industry which illustrate some of the above mentioned topics. It was clear from the onset that it will be impossible to produce an all-encompassing overview covering all application areas and available software tools. For the sake of clarity, the focus of this issue was directed towards structural applications. Maybe a future edition of the GACM-report can focus on other simulation disciplines and codes.

The major software vendors in the structural field were invited to submit a contribution and many thanks go to all those who followed the call. It would be a great reward if this edition would be a small puzzle piece towards bridging the gap between industry and academia.

July 2015
Thomas Münz
DYNAmore GmbH
Stuttgart

Message of the President

The objective of GACM, according to our bylaws (see www.gacm.de/bylaws/), is to stimulate and promote education, research and practice in computational mechanics and computational methods in applied sciences, to foster the interchange of ideas among various fields contributing to computational mechanics, and to provide forums and meetings for the dissemination of knowledge about computational mechanics in Germany. Most of our visible activities have circled around research so far. But many members and officers of GACM are also very much concerned about the other two aspects, namely education and practice. We currently think about dedicating one of the next issues of GACM report to the field of education. But this issue, like Report No. 4, focuses on the application side. I am very happy that Thomas Münz, member of our Executive Council (EC), volunteered to edit this issue and was able to stimulate a number of very interesting articles from the industrial side. This should help the current GACM EC in its effort to bring academia and industry together …

It takes two to Tango

Academia and Industry – a never ending (love?) story (of misunderstandings?)

Since many years I have witnessed countless discussions on the relation between academia and industry. Nobody on either side ever really doubted the importance of the other one. But at the same time I haven't found too many people that have been satisfied with the status quo of this relationship. One can find all levels of haughtiness on both sides but sometimes also different kinds of (hidden) inferiority feelings. I am convinced that both sides would heavily benefit from better collaborations and an open exchange of thoughts. And even more, I am convinced that not even the status quo will stay if we allow this widening gap to continue to grow. Academia more and more needs to leave the ivory tower (which anyhow isn't ivory anymore) and take up the real world challenges once their research is advanced enough. And people in industry more and more need to question their current "Gold standard" and risk using new ideas and methods, because it might give them the biggest advance compared to their competitors … maybe not tomorrow, but already in the medium-term and sooner as they fear. So let's start finding new ways of openly talking to each other. Let's have joint meetings without hidden agendas, i.e. no meetings to just get some more project funding and then don't care about the usable outcome and no collaborations to just get cheap labor because the brilliant co-worker gets some extra payment in the form of a PhD degree. But instead, work together to really show what Computational Mechanics can do nowadays – for industry and for society. Most people will be quite surprised to see what really can be done, and at which sophisticated and mature level, if we combine the best of both worlds. But this cannot be changed by a decision of the EC of GACM. But GACM might be able to provide a useful platform and foster any initiatives in this direction. So my wish for all of you again is: get involved!

Wolfgang A. Wall

Visit our New Website

At the last general assembly during WCCM 2014, the German Association for Computational Mechanics (GACM) proudly presented the new website *www.gacm.de* to its members. Some weeks later, this new official gateway to all GACM activities went online for the general public. The GACM Executive Council would particularly like to thank our Secretary General, *Alexander Popp (TU Munich),* for his dedication and tireless efforts to put the idea of a new contemporary website into practice.

The new website www.gacm.de comes with a contemporary design and layout.

Both GACM members and visitors interested in computational mechanics research in Germany and abroad will receive miscellaneous information services on *www.gacm.de*. Among the most important is an overview of recent, current and future GACM activities, such as the *GACM Colloquia for Young Scientists,* the news bulletin *GACM Report,* different awards conferred by GACM and other events or initiatives, such as the *3rd German-Japanese Workshop on Computational Mechanics* held in Munich on March 30-31, 2015.

There are also dedicated subpages presenting the members of the GACM Executive Council, the 25-year history of our association and the scientfic network into which GACM is embedded. As a special service to the young members of our community, GACM currently works on establishing a new job database with job openings in the field of computational mechanics (education, research and practice) in both Germany and all over Europe. It is also planned to further expand the associaion's activities for young researchers, which will be done in close collaboration with the *ECCOMAS Young Investigators Committee*.

Last but not least, the success of a scientific association largely depends on the dedication and commitment of its members. This why the new website comes with an entirely new *Members Area,* which will serve as first contact point for all GACM members. After logging in, our members have access to internal news and a download section, and they can administrate their membership data with an easy-to-handle set of web forms. Those interested in becoming a member of GACM (student, personal or corporate memberships are available) are invited to visit the *Membership* section, which contains all necessary information regarding the benefits and membership fees as well as an online application form. Get involved!

Frequently asked questions (FAQ)

Some frequently asked questions concerning the new website and GACM membership.

Q: I have an academic opportunity available in my group (e.g. PhD or Postdoc). Can I call attention to this job opening through the GACM website?

A: Yes. The new GACM job database has been launched precisely

for this purpose. Please log-in to the ➢*Members Area* and choose the menu item ➢*Open Position*. All we need is a PDF file of your job description.

Q: I am interested in learning more about other GACM members and getting into contact with them. Does the GACM website offer any help?

A: Yes. Have a look at our ➢*Member List*, where many members provide links to their personal or professional websites. If you would like to provide a link yourself, just log-in to the ➢*Members Area* and choose the menu item ➢*My Data*.

Q: I would like to read the GACM Report in electronic format. Are these available on the new GACM website?

Dedicated subpages for each topic: e.g. GACM News, GACM Report and our Members Area.

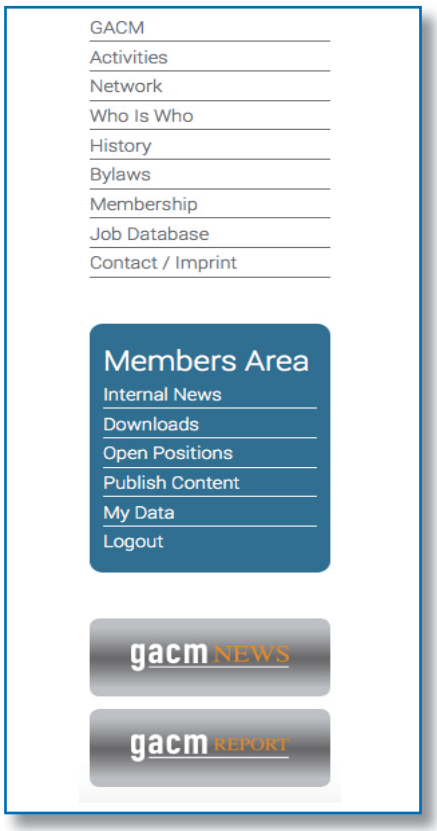

Easy navigation through all website contents using the GACM sidebar menu.

A: Yes. All GACM Reports ever published can be downloaded from our ➢*Members Area* by clicking on the menu item ➢*Downloads*. You can also find protocols of the last GACM General Assemblies, the official GACM logos and other documents there that might be helpful for you.

Q: I am planning to register for a conference, where ECCOMAS members are entitled to a reduced conference fee. Can I obtain an up-to-date GACM membership certificate? How does it work to get this certificate?

A: Yes. As a GACM member, you can now download a membership certificate at any time. Just log-in to the ➢*Members Area* and choose the menu item ➢*My Data*. The certificate is generated automatically and can be used straightaway.

Q: My affiliation and my address have changed. Do I have to send a letter to the GACM office to have these changes registered?

A: No, with our new website things are much easier. You can administer your entire membership data online. Just log-in to the ➢*Members Area* and choose the menu item ➢*My Data*. Your new data will be activated within a few working days.

Q: I still pay my GACM membership fee by an annual bank transfer. Can I reduce my administrative efforts by participating in GACM's automatic debit transfer system (‚Bankeinzug / Lastschriftverfahren')?

A: Yes, we strongly encourage you to participate in our automatic debit transfer system, since this minimizes not only your but also administrative efforts with regard to membership fees. To do so, you can simply download a so-called SEPA authorization form from the ➢*Downloads* section in our ➢*Members Area*. Please fill-in, print and sign this form and then send it to us.

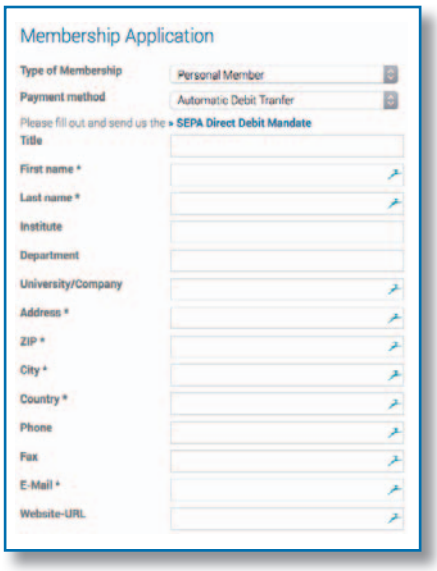

New members can apply easily with the GACM online application form.

Status on State of Art Simulation with PEM Methods in the Automotive Industry

A. Caillet and D. Blanchet
ESI Gmbh, Ascheim/München, Germany

Abstract

During the last decade, big progresses were made on software and hardware sides allowing an efficient use of PEM elements to represent explicitly the trims for the FEM simulation of full vehicles. Representing the trims as PEM elements in FEM vehicle models allows a more accurate description of the physical behavior up to 400Hz for structureborne excitations compare to the classical method using the non structural masses and high values of damping in the fluid domain which shows limitation after 200Hz.

This paper will make a overview of the state of the art technics for modelling porous and elastic trims with PEM through the existing literature in the automotive industry. The focus will be made on the full vehicles scale interior acoustic for structureborne excitations and on component scale for the analysis of transmission loss. The paper will discuss about the most commonly accepted meshing rules. The effect of the boundary conditions on the results will also be studied.

1 Introduction

Limitations are met by the two classical methods to model trims in NVH simulation models. To avoid these limitations and describe with a higher degree of detail the trims included in the vehicles the FEM-PEM method is a good choice. This method uses a (u,p) formulation developed by reseachers giving the opportunity to the engineers to study more into details the effects of the poro-elastic trims on the vibro-acoustic response of the full vehicle or a component to a structureborne or airborne excitation.

2 Classical modelling methods for trims

2.1 Non-structural masses and high damping value

The most classical modelling method for the trims in full vehicle FEM models consists in 2 parts: first to model the effect of the trims on the structure, the trim masses are smeared on selected parts of the structure as non-structural mass This method will take account of the transmission effect of the trim through its assuming that the trim has a constant thickness over the selected parts. The damping added to the structure by the visco-elastic behavior of the foam parts is not included here. Local masses are also added to the structure to model trims which are attached at certain points of the structure. It is usually the case for the door panels, headliners, trunk trims. A second part is related to the acoustic domain. A high damping is set to the acoustic cavity to account for the absorption effect of the trims. Damping value is in that case between 10 and 20%. These methods are suitable to get an idea of the effects of the trims up to 200Hz [10]. But it reaches its limits when it is question to go higher in frequency or analyses in detail the local effect of the trims. No local behavior of the trim can be investigated with this method.

2.2 Trims as TMM

The transfer matrix method provides also the possibility to model the trims. Duval and al. have shown in [1] that: " … the TMM (Transfer Matrix Method) was giving excellent results for flat samples with spatial windowing but was not at ease with curved shapes due to the decrease of Insertion Loss slopes of insulators with curvature [2], [3]. First 3D investigation on a simplified trimmed half-cylinder structure using poroelastic trim FEM modeling in the low and middle frequency gave promising results and proved that this approach was necessary to catch the three dimensional coupling effects between structures and trims.

3 Theoretical background

3.1 Porous material modelling

As described in [13],[14],[15], propagation of elastic and acoustic harmonic waves, with an $e^{-i\omega t}$ time dependency, in porous elastic media is governed by the following system of modified Biot's equations:

$$\tilde{\rho}_s\,\omega^2 U + \mathrm{div}\left(\sigma^s_{kl}(U) - \tilde{\alpha}\phi\, p\,\delta_{kl}\right) + \tilde{\beta}\,\mathrm{grad}(\phi p) = 0 \quad (1)$$

$$\mathrm{div}\left(\frac{1}{\omega^2\tilde{\rho}_f}\mathrm{grad}(\phi p) - \tilde{\beta}U\right) + \frac{\phi p}{R} + \tilde{\alpha}\,\mathrm{div}(U) = 0 \quad (2)$$

Where: The vector U represents the skeleton displacement, σ^s_{kl} the components of the stress tensor in the skeleton and p the acoustic pressure. $\boldsymbol{\omega}$ is the angular frequency, $\boldsymbol{\Phi}$ is the porosity and $\tilde{\rho}_s, \tilde{\rho}_f$ are respectively the skeleton and fluid equivalent mass densities, which are related to the real mass densities ρ_s, ρ_f of the structure and fluid by:

$$\tilde{\rho}_s = (1-\phi)\rho_s + \phi\rho_f\left(1-\frac{\rho_f}{\rho_e}\right) \quad (3)$$

$$\tilde{\rho}_f = \phi\rho_e \quad (4)$$

Where ρ_e is the effective mass of the interstitial fluid given in [15]. Equation 5 represents the inertial coupling factor and equation 6 represents the stiffness coupling factor.

$$\tilde{\beta} = \frac{\rho_f}{\rho_e} \qquad \phi\tilde{\alpha} = 1-\frac{K_b}{K_s} \quad (5,6)$$

The coefficient R represents the bulk modulus of the porous elastic media.

$$R = \frac{K_s\phi^2}{1-\phi-K_b/K_s+\phi K_s/K_e} \quad (7)$$

The coefficients Kb, Ks represent respectively the bulk modulus of the skeleton with vacuum inside and of the material of the skeleton, and finally Ke represents the effective bulk modulus of the interstitial fluid as given in reference [15].

3.2 Biot parameters identification

Ten years ago, only few engineers had the opportunity to work with Biot parameters. Just a handful of laboratories were able to provide these values based on extensive sophisticated measurements. Fortunately, today's situation has drastically changed. Biot parameters can be identified using an indirect method. Based on a simple impedance tube measurement (Figure 1) and the measurement of acoustic porosity and air flow resistivity which can now be determined experimentally with reasonable accuracy, the acoustic Biot parameters (Φ open porosity, σ static airflow resistivity, α∞ geometrical tortuosity, λ viscous characteristic length, λ´ thermal characteristic length) can then be calculated using different optimization algorithms [10],[17],[18]. These identified Biot parameters are the intrinsic properties of the poroelastic properties because only one set of parameter values is possible in the solution. To fully characterize foam type material extra properties such as Young's modulus and damping of the foam structure is needed. These are easily obtained from a quasi-static mechanical test. Figure 2 shows the sensitivity of the different Biot parameters over the frequency range.

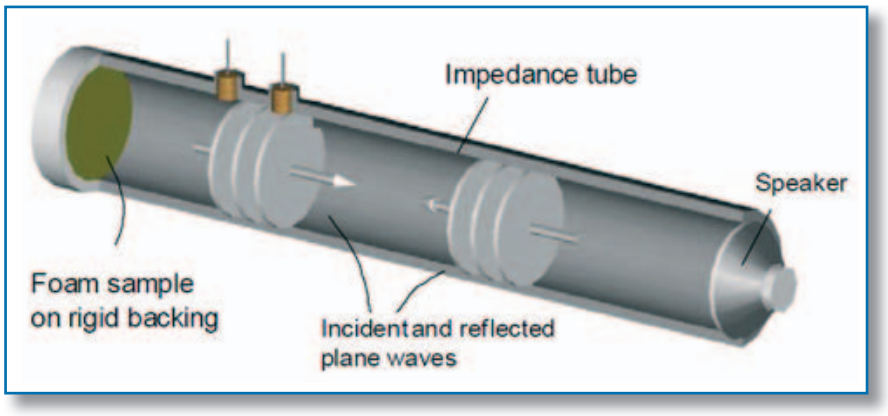

Figure 1: Impedance tube

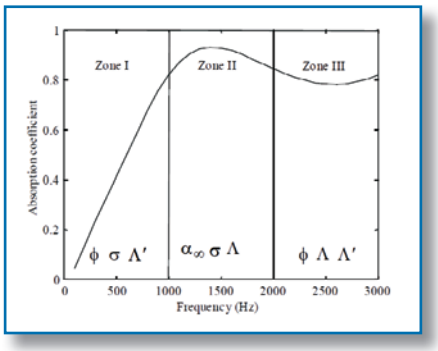

Figure 2: Frequency zones of a typical Biot parameter

3.3 Full vehicle modelling

As described in Figure 3, the trim of a full vehicle analysis can be added to the classical structure/fluid coupled linear system as a trim impedance matrix $\tilde{Y}$. The dynamic equation of the trimmed vehicle can be written in the following form:

$$\begin{bmatrix} Z_s & C_{sc} \\ C_{sc}^t & A_c \end{bmatrix} + \begin{bmatrix} \tilde{Y}_{ss} & \tilde{Y}_{sc} \\ \tilde{Y}_{sc}^t & \tilde{Y}_{cc} \end{bmatrix} \begin{bmatrix} U \\ P \end{bmatrix} = \begin{bmatrix} F \\ Q \end{bmatrix} \quad (8)$$

Where Zs is the mechanical impedance of the master-structure (car body in white), Ac is the acoustic admittance of the internal cavity. Csc is the surface coupling operator between the untrimmed master-structure surfaces directly in contact with the internal acoustic cavity.
U is the displacement field vector of the master-structure, P the pressure field of the internal cavity; F the external force field applied to the master-structure, and Q represents internal acoustic sources. The matrix $\tilde{Y} = R'YR$ is the transferred impedance matrix of the porous component where R is the transfer operator relating the degrees of freedom of the porous component to the degrees of freedom of the master structure and of the internal cavity.
The linear system of equations (8) is solved using structural and acoustic normal modes. This has the great advantage of keeping the trimmed linear system to be solved at the same size as the initial BIW linear system.

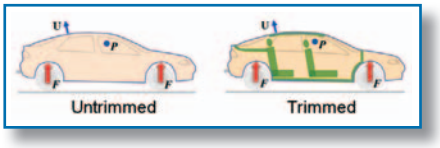

Figure 3: Untrimmed and trimmed configuration

3.4 Transmission loss

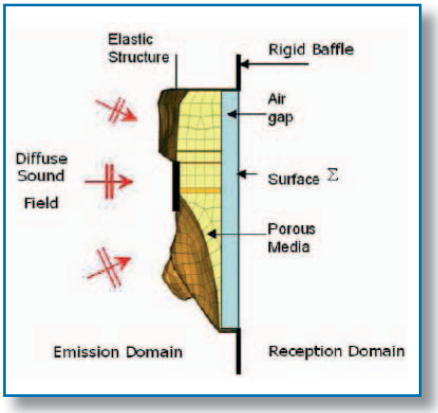

Figure 4: FEM/BEM/PEM Transmission loss model setup

As described in [4] the implementation of the Transmission Loss (TL) computation is based on FEM-BEM method allowing calculation of the acoustic TL of a double wall trimmed component of arbitrary shape, involving in particular the use of poro-elastic materials (foams, fibers, etc..) between structural outer panels with or without air gaps (see Figure 4). Theory used for TL modelling is based on displacement/pressure formulation (u,p) proposed by Atalla et al. [13,14]. This formulation has been extended to study vibro-acoustic problems involving interactions between a master structure, a fluid cavity and trim components made of poro-elastic material. This formulation has been implemented into VTM and details of this formulation are given in [5,6]. Complex industrial applications require the modelling of interactions between porous media and infinite fluids of the emission and reception rooms. The method proposed consists in adding an air gap between the porous media and the infinite fluid. On the coupling surface ∑ separating the air gap and the external fluid (see Figure 4), two boundary conditions are defined: a) continuity of pressure: $p^g = p^e$ and b) continuity of normal displacement: $u_n^g = u_n^e$ Symbols g and e denote respectively the air gap and the external fluid. The weak formulation of the porous media including the air gap is given by: (9)

$$Z(U,V) + A(p,q) - \hat{C}(p,V) - \hat{C}(q,U) = \tilde{C}_s(T,V) + C_s(q,\varphi(U_n^f - U_n))$$

Where, Z represents the mechanical impedance of the skeleton, A represents the admittance of the interstitial fluid and the air gap, Ĉ represents volume coupling terms between the skeleton and the interstitial fluid, s C_s represents surface coupling term between the porous media and the elastic structure, s C represents surface coupling terms between the porous media, the air gap and the external fluid. The use of this formulation combined with integral representation of pressure in the emission and reception domains and the use of the boundary conditions defined above enables the creation of a linear matrix system that yields Transmission Loss values of the component. The full theoretical background can be found in [4,7].

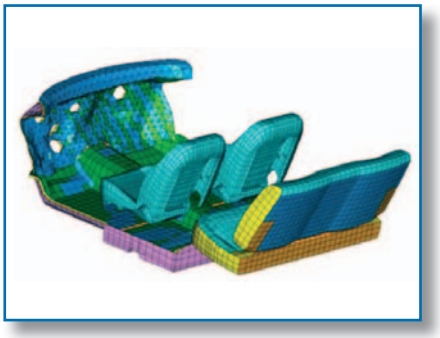

Figure 5: Anciant and Al, interior trim models

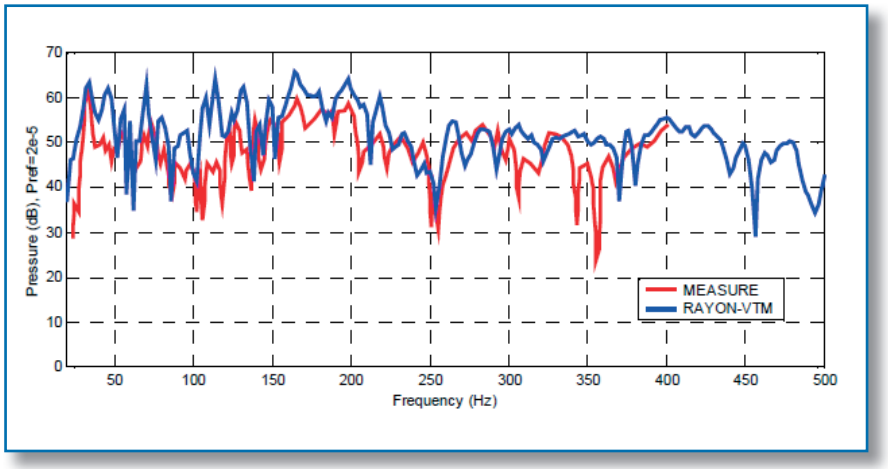

Figure 6: Anciant and Al, SPL correlation at driver's head

4 Application

4.1 full vehicle

[1] In 2007, Anciant and al in [2], [3], [4], [5] analyzed the correlation between measurements and simulations for a fully trimmed vehicle. In this case, all the porous trims (seats, carpet, dash insulator…) are represented as PEM elements (Figure 5). A relatively simple representation of the trims using quadratic solid elements was done. A good correlation is observed at several microphones up to 400Hz. On Figure 6, the microphone located at driver's head is displayed. The model could be computed within a reasonable time of a night.

Between 2007 and 2014, many improvements have been done on the software implementation (in terms of parallelization, modular approach for the computation of the trim impedance matrices…) and the hardware allowing the creation of much more detailed models. Since 2012, the PEM element formulation is integrated in ESI group

VPS software [19] allowing a much more efficient use of the hardware and giving the possibility to compute more detailed models and get more output possibilities (Operational deformation shapes, contour plot for displacements in structure and trims and pressure for trims and the acoustic cavity.

In 2011, Henrich and al. in [9] investigated the differences between the measurements different methodologies to model the trims in a full vehicle FEM model: the classical methods to model trims: trims as non-structural masses with a global acoustic damping value (basis NSM in orange), trims as non-structural masses with surface absorption on the cavity (NSM Var49) and trims as PEM (VTM in blue). Figure 7 shows the correlation between the different methods at Driver's head microphone. It can be seen that the curve obtained with the FEM-PEM method (VTM) follows better the trend of the measurement curve than the other methods.

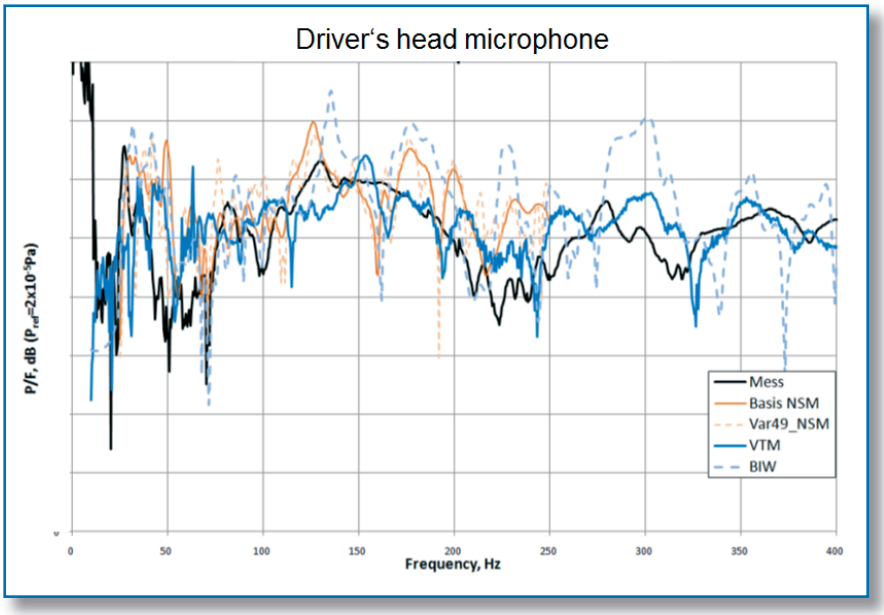

Figure 7: Henrich and Al, SPL correlation at driver's head, comparison between the different methods

In 2014, Caillet and al in [10] presented a much more detailed model to study the influence of the porous trims (dash insulator, carpet, headliner, seats…) and the influence of the plastic trims (like trunk trim panels, pillar trims package tray) on the response of a full vehicle trimmed body model to a structureborne excitation. A total of 600739 PEM quadratic elements are used in the model (Figure 8). All the different layers describing the trims are created with a special care in the mesh to account for the thickness spatial dependency. An element size of 30 to 40mm was chosen to model the different trims.

The influence of the boundary conditions has been studied for the case of the connection of a plastic trim with the structure. A difference of up to 10dB is observed in the results (Figure 9). Different boundary conditions are currently available in VPS to model the coupling of the trims with the structure and the acoustic domains ([19]). On the Driving point inertance, almost no difference is seen as the trim is considered light and very flexible compare to the structure. On the SPL results at a microphone located in the trunk, a difference is seen. As the trim selected (trunk trim) is made of rigid plastic, it can be expected that the plastic panel is radiating energy differently to the interior acoustic cavity. The coupling conditions have to be defined like in reality. An influence on the response can be observed when one of the trims (trunk trim) is removed from the model (Figure 10). A similar behavior to what was seen for the case of modifying the boundary condition can be seen in that case. Removing the trunk trim has almost no influence on the driving point inertance but a different is seen on the pressure at the driver's head microphone showing an improvement of the SPL when the trim covers the wheelhouses. The classical method using the non-structural masses to model the trim would not have given the opportunity to investigate such problematics like modifying the coupling conditions of the trims to the structure/acoustic domains or adding/removing a part. Having the flexibility to modify the model and check its sensitivity to the modification is one of the advantages of the method despite a longer modeling time.

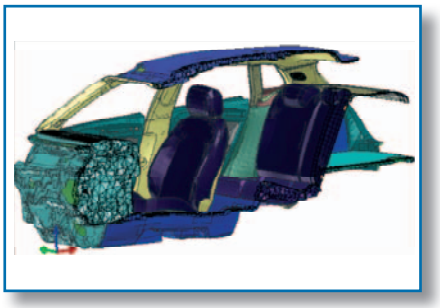

Figure 8: Caillet et al, Interior trims included in model

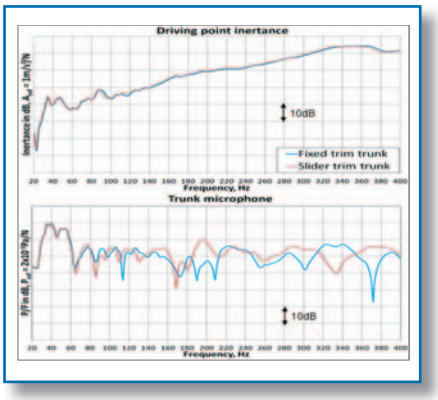

Figure 9: Caillet et al, Influence of structural boundary conditions

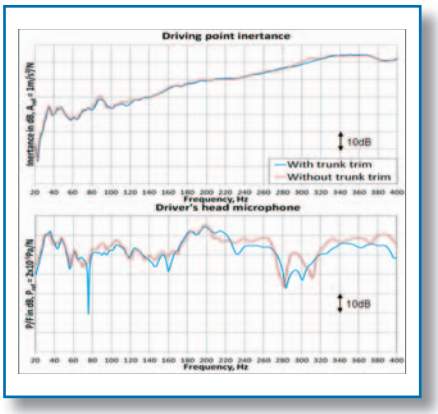

Figure 10: Caillet et al, Influence of removing the trunk trim

4.2 Transmission loss

In 2007 Mebarek and al. [20] studied the modelling of a dash insulator using the FEM/BEM/PEM method. A PEM model of the dash insulator was created. The different layers of the trim (porous material, heavy layers, fibers) are represented explicitly in the model with solid elements. For each layers of material more than one layer of elements can be used depending of the thickness of the layer in reality. The model is illustrated in Figure 11 2 types of dash insulator concept have been implemented in the model and compared with the measurement (config A: 2 felt layers, Config B: felt/Heavy layer). A very good agreement can be seen between the measurement and the simulation on Figure 11. The benefit of using the trim can be clearly seen on the graph. The sensitivity of the model is also well predicted.

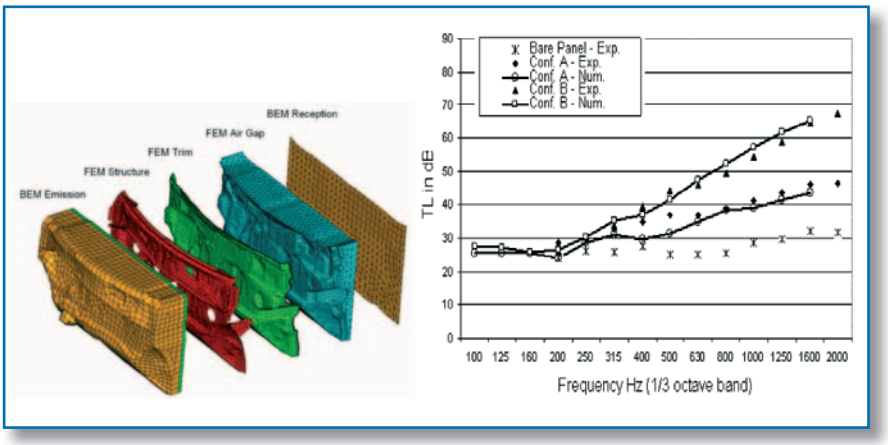

Figure 11: Mebarek et al, FEM/PEM/BEM TL simulation vs measurements

Rondeau and al. [21] studied the influence of integrating the instrument panel within the transmission loss model. The instrument panel is integrated in the model with PEM elements. Its influence will be taken into account within the impedance matrices computed from the PEM elements. The sensitivity of the model to the addition of the instrument model is the same as the reality. Figure 12 illustrates the integration of the instrument panel and the sensitivity of the model to the modification.

5 Conclusion

The PEM method is a very good way integrate poro-elastic trims in FEM models. This method allows realistic prediction of influence of the trims for a full vehicle model or a component. Engineers can rely on it to investigate new virtual trim concepts instead of creating several prototypes.

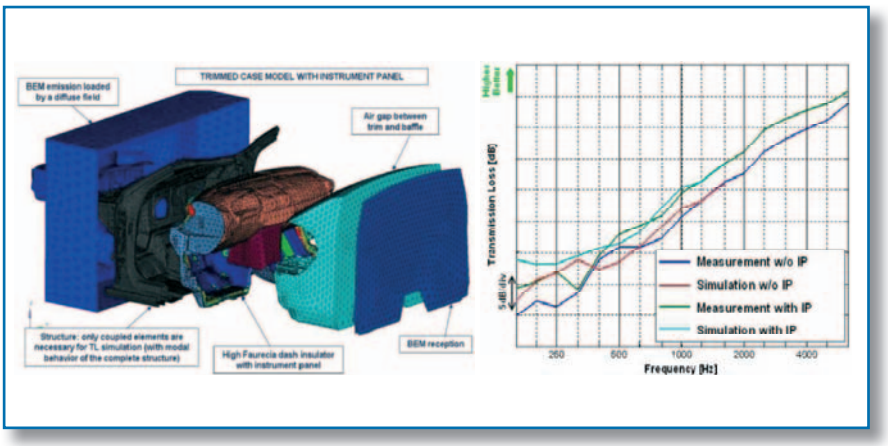

Figure 12: Rondeau et al, FEM/PEM/BEM TL simulation vs measurements, include cockpit in model

www.esi-group.com

References

[6] A. DUVAL and al.: "Trim FEM simulation of a dash and floor insulator cut out modules with structureborne and airborne excitations", In Euronoise-Acoustics'08, Paris, France, 2008.

[7] A. Duval and al. "Faurecia vehicle acoustic synthesis method: A hybrid approach to simulate interior noise of fully trimmed vehicles", Congrès SIA Confort automobile et ferroviaire 2004, Le Mans.

[8] A. Duval and al. "Vehicle acoustic synthesis method 2nd generation: an effective hybrid simulation tool to implement acoustic lightweight strategies" Journées SFA/Renault/SNCF, Guyancourt, 2005

[9] A. Omrani, L. Mebarek and M.A. Hamdi, "Transmission Loss Modeling of Trimmed vehicle Components", ISMA, (2006)

[10] M.A. Hamdi, L. Mebarek, A. Omrani, N. Atalla, M. Fortez, G. G. G. Crignon, S. Lullier, "An efficient Finite Element Formulation for the analysis of Acoustic and Elastic Waves propagation in Sound Packages". SAE 2001, 01 NVC -165.

[11] C. Zhang, M.A. Hamdi, L. Mebarek & B. Mahieux, « Influence of porous elastic components on structure and air borne noise in low and medium frequency ranges », Rieter Automotive Conference June5th-7th (2005)

[12] A. Omrani, D. Blanchet and Hideki Niwa, "Theoretical Foundation for the Modeling of Transmission Loss for Trimmed Panels". Presented at 2007 JSAE Congress.

[13] M. ANCIANT and al.: Full trimmed vehicle simulation by using Rayon-VTM., In JSAE, Japan, 2006.

[14] B. Henrich and al, "Using VTM (Vehicle Trim Modeler) to Represent Acoustic Trim Effect on Full Vehicle Level", VAUC2011, Sindelfingen, 2011

[15] A. Caillet and al, "Prediction of Structureborne Noise in a Fully Trimmed Vehicle using Poroelastic Finite Elements Method (PEM)," SAE Technical Paper 2014-01-2083, 2014, doi:10.4271/2014-01-2083.

[16] D. Blanchet and al.: "Modeling the vibroacoustic effect of trim on full vehicle and component level analysis", DAGA, 2009

[17] D. Blanchet and al.: "Acoustic trim modeling: traditional spring/mass system vs Biot theory", EAA Euroregio Ljubjana, 2010

[18] N. Atalla and al.: "A mixed pressure-displacement formulation for poroelastic materials" J. Acoust. Soc. Am., 104(3), 1444-1452., 1998

[19] N. Atalla and al.: "Enhanced weak formulation for the mixed (u,p) poroelastic equations" J. Acoust. Soc. Am., 109(6), 3065-3068., 2001

[20] Allard, J. F.: "Propagation of Sound in Porous Media, Modelling of sound absorption", Charpman & Hall, North Way Andover, Hampshire, SP105BE, England, 1993

[21] Y. Atalla, R Panneton: Inverse acoustic characterization of open cell porous media using impedance tube measurements, Canadian Acoustics, Vol 33 No.1, 2005

[22] R. Panneton and al.: Blanchet D., Bloor M., Validation of the Inverse Method of Acoustic Material Characterization, SAE2003, 2003-01-1584, 2003

[23] FOAM-X User's guide

[24] ESI VPS Solver reference guide

[25] Mebarek et al, Modelling of Transmission loss for trimmed vehicle component VTM TL, JSAE, 2007

[26] Rondeau, J., Dejaeger, L., Guellec, A., Caillet, A. et al., "Cockpit Module Analysis Using Poroelastic Finite Elements," SAE Technical Paper 2014-01-2078, 2014

Technology Symbiosis of Topology Optimization and Additive Manufacturing Enables Weight Savings of up to 60 Percent

M. Bromberger
Altair GmbH, Böblingen, Germany

Additive Layer Manufacturing (ALM) gives the engineer a new dimension of freedom in component design; gone are the constraints of traditional manufacturing and free-form design is now possible. Key enabler to allow the engineer or designer to explore this design freedom is topology optimization. The technology symbiosis of additive manufacturing and topology optimization enables engineers to push the boundaries and produce truly optimal designs. Many designers and engineers are still thinking in classic manufacturing pattern as they are not yet used to new manufacturing methods such as additive manufacturing, which requires them to rethink the development process. A better knowledge of material properties used within additive manufacturing is required to ensure efficient design of components. For every process it is important to understand its details and to know the process parameters to simulate and predict the component's behavior.

Altair, a renowned software and engineering services provider, has an in depth, 20 year experience in topology optimization. The company provides tools such as OptiStruct, part of Altair's CAE Suite HyperWorks, and Inspire, developed and distributed by Altair's subsidiary solidThinking. With its consulting department ProductDesign Altair also supports its customers in applying these technologies in their development processes, supporting a simulation driven design process. With topology optimization tools such as OptiStruct and Inspire as well as initiatives such as Optimization Centers, Altair enables its customers to develop lighter and better performing products.

Renishaw, an established world leader in engineering technologies, with a strong history of innovation in product development and manufacturing has deployed topology optimization and additive manufacturing to develop and manufacture innovative products that are lighter and/or stiffer than traditionally developed and manufactured products. Renishaw's laser melting process is an emerging manufacturing technology with a presence in the medical industry as well as the aerospace and

high technology engineering and electronics sectors. Laser melting is a digitally driven additive manufacturing process that uses focused laser energy to fuse metallic powders into 3D objects. One of Renishaw's latest project was the development and manufacturing of a 3D printed bike for and with Empire Cycles.

Inspire in the Design Process

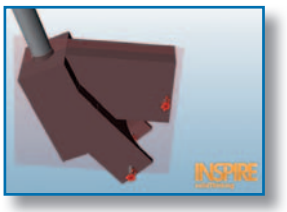

Chris Williams from Empire Cycles had been using additively manufactured components in production for many years, but wanted the opportunity to test the method on a full working product. He contacted Renishaw and explained what he wanted to do. The team at Renishaw thought that some of the standard simple parts of a bicycle like the seat post or headstock would be the best fit to shave off a few precious grams of weight, as these were known entities and simple enough to validate and test. Professional road racing teams place significant investment into losing a gram of weight here or there, gaining a split second in the process.

Renishaw used solidThinking Inspire to perform concept generation and topology optimization to generate an optimum design solution for the bikes seat post. A tool such as Inspire goes hand in hand with ALM by generating component designs that maximize the manufacturing freedom of ALM, leading to stronger and lighter components that can often not be produced with traditional manufacturing techniques.
The original CAD data was imported into Inspire. Retaining bolts and seat post were modelled. This enabled the retaining bolts to be fixed and acting forces applied to the end of the seat post. The bounding area was maximized to give Inspire maximum design freedom. Next, the optimized design was generated with Inspire. Then a second iteration was carried out using a smaller design space drawn around the area generated by the first optimization. The new material layout generated by Inspire provided a concept that not only met the performance targets but was also minimum mass. Chris Williams then took this model and used his own design know-how to generate suitable geometry around this concept for ALM manufacture.

The Results: Stronger and Lighter Designs

The ultimate aim of the project was weight saving, and the resulting parts are designed for maximum strength with minimum weight. "We took the seat post bracket from 360 grams down to 200 grams, and the cost of the weight savings don't have to be made up in other areas," explained Robin Weston, Renishaw Marketing Manager.
Further weight was saved by integrating the clamping threads into the design, doing away with the need for a separate bracket. With the huge weight saving achieved on this single component, the scope suddenly expanded.
"Where we'd thought about extruded or hydroformed aluminum tubing or even carbon fiber for the frame, bonded onto some titanium bits, we started to look at doing even more. Chris Williams explained that the use of the standard frame materials really inhibited the design freedom. As we looked at the likes of the main aluminum frame and realized that component weighed 2100 g on its own; we knew we could help to create something equally as strong and shave a huge amount of the weight off. From there the idea that we could use additive manufacturing to create all of the major frame components came together".

In terms of strength the initial optimized seat post bracket has already been tested to the BS standard, which includes exerting 1,200 newton applied and released for 50,000 cycles at no more than 25 hertz.
"We thought why not test to destruction and see how strong it really is – so far it has exceeded the standard 6 times, at 300,000 cycles and counting. This is after stress relief only; we are planning advanced heat treatments, such as Hot Isostatic Pressing (HIP) which could improve the properties even further".

What's Next

The benefits of the interaction between topology optimization with solidThinking Inspire and additive manufacturing are obvious. Topology optimization tools such as Inspire or OptiStruct offer the best way to create load specific structures and enable the industry to unlock the enormous lightweight design potential related to use of additively manufactured structures.
It is very beneficial to create and design additively manufactured components with topology optimization, since the weight saving potential is enormous. By combining the two technologies, weight savings of up to 60% can be achieved. Compared to traditionally manufactured parts and the ongoing development of both simulation and additive manufacturing this approach promises enormous cost savings, even with this so far relatively cost intensive production method.

www.altair.de

Excellent Brake Noise Comfort by Simulation – Advanced Methods to Create Stability Maps

S. Carvajal Gonzalez[1], D. Wallner[1], R. Helfrich[2] and M. Klein[2]
[1]Porsche AG, Stuttgart, Germany, [2]INTES GmbH, Stuttgart, Germany

Abstract: Numerical methods for brake squeal analysis are widely accepted in industry. The approach to use complex eigenvalue analysis is successful to forecast the appearance of squeal noise. Using simulations in an early design stage helps to reduce time to market, to save costs and to improve the physical behaviour and robustness of the system. This paper will show advanced methods that use a specific strategy to reduce computation time. The industrial example of a PORSCHE brake system is analysed by this simulation strategy. The process starts with the validation of the disc by comparison of mode shapes from test rig with FEM results and subsequent geometrical optimization. The next step is model updating of the transversely isotropic material of the pad. All remaining parameters, like brake pressure, rotational speed of the wheel, friction coefficient between disc and pad, and Young's modulus of disc are samples in one single PERMAS run. The resulting stability map expands the knowledge about the NVH behaviour and robustness of the brake system for a wide range of parameter combinations. The additional information from the stability map strongly supports the development of a robustly quiet brake system.
Keywords: Brake squealing, complex eigenvalues, sampling, stability map, high performance

1. Use of Simulation in Industry

Simulation methods for brake squeal analysis are widely used in industry. The complex eigenvalue analysis (CEA) as implemented in PERMAS with special extensions for improved accuracy and high performance is successfully applied by PORSCHE AG to predict squeal noise (see Fig. 1). Using simulations in an early design stage helps to reduce time to market, to save costs and to improve the acoustic behavior and robustness of the brake system.

The first step in CEA is a static contact analysis, which takes into account friction, brake pressure, vehicle speed and moment of inertia due to rotation as well as any pretension, which is applied in the brake system by bolts or other means. The resulting contact status is used to linearize the nonlinear contact problem in order to proceed with modal dynamic methods.

The second step is the calculation of real eigenvalues. Additional stiffness effects are taken into account due to rotation and contact.

The third step is the calculation of complex eigenvalues. Here, the gyroscopic effect and additional damping due to contact is included in addition.

The fourth step is sampling, which will be explained in the subsequent sections of this paper.

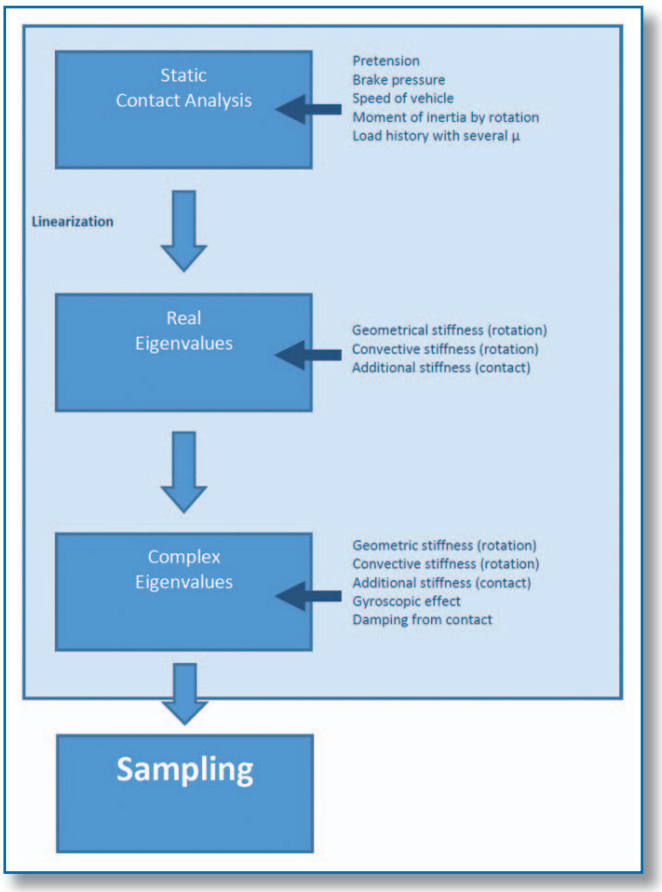

Figure 1: CEA with Sampling

2. State of the Art

Today's state of the art in brake squeal analysis is best characterized by performing one calculation run for one operational point with one set of parameters [1, 2]. Some of these brake system parameters could be determined in advance, e.g. by measurement, and will show only little change during brake operation. However, the brake system has an infinite number of operating points and many parameters with a wide spectrum of possible values. Due to wear of pads and disc some parameters change during lifetime of the brake system. Typical parameters are brake pressure, fric-

tion coefficient between disc and pad, and vehicle speed. Another group of parameters depends on conditions during production. A typical example for this group are material parameters.

3. Sampling by Simulation

It is an important target of brake development to create a brake system with a high robustness for several parameter sets. The key for that target is a stability map created by simulation (Fig. 1). If the established analysis procedures are simply repeated with several parameter sets, computing time would drastically grow with every additional parameter. Therefore, advanced time saving approaches are required to create such a stability map in acceptable run times. Such time saving approaches for the sampling method were developed and implemented in PERMAS.

4. Step 1: Stability Map to Understand System Behaviour

Sampling is performed for a brake system (Fig. 2) of a series production vehicle of Dr. Ing. h.c. F. Porsche AG.

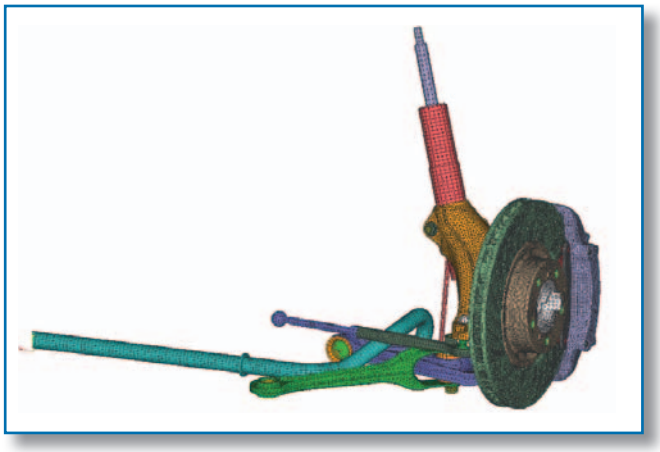

Figure 2: Brake model of a series production vehicle of Dr. Ing. h.c. F. Porsche AG

The development objective of the simulation is the design of the brake system with a high robustness for several parameter sets. The example model has 2,107,320 degrees of freedom and 18,852 contact degrees of freedom. There, 219 real eigenvalues and 240 complex eigenvalues are calculated. The following parameters are used with the new sampling method:

- 79 rotational speeds from $\omega = 1$ to $\omega = 40$ [rad/s] in 0.5 rad/s steps.
- 3 Young's moduli for the brake disc E = 96, 105 and 120 [GPa].
- 30 coefficients of friction between pad and disc from $\mu = 0.3$ to $\mu = 0.9$.

With the conventional method (79 * 3 * 30 =) 7,110 runs of the solver were needed.

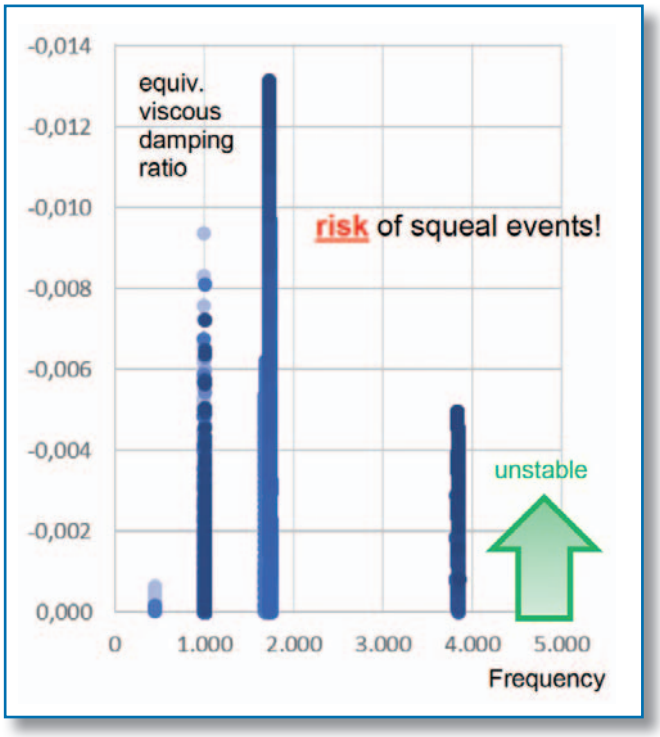

Figure 3: Stability map based on 7,110 results

Fig. 3 shows the stability map with the equivalent viscous damping ratio over frequency for the 7,110 sets of parameters. There, only the negative values are shown, because they indicate the risk of squeal events. The larger the negative value, the higher the risk of squeal events. The stability map gives an overview of the squeal behaviour. At three frequencies, potential squealing is identified (about 1000 Hz, 1700 Hz and 3800 Hz). At 1000 Hz, there is only a small change in frequency, and only some parameter sets indicate a high risk of squeal events. A split into two frequencies exists at about 1700 Hz. A stronger dependency on the various parameter sets is present at about 3800 Hz.

The stability map is generated using all results from 7,110 samples, which are all calculated by one single computation run in about 5 hours on a single compute node.

Based on the stability map, the highest risk of squeal events is seen around 1700 Hz. A detailed analysis of this frequency range is easy, because all data required are already available. Hence, the dependency from each parameter can be extracted easily and without additional computational effort. In Fig. 4, the equivalent viscous damping ratio is on the ordinate as before and the abscissa represents the rotational speed in both charts.

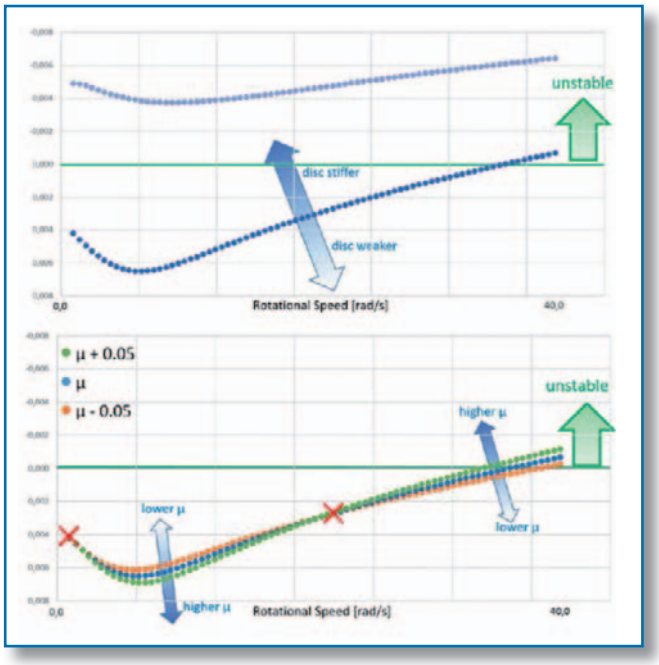

Figure 4: Change of the equivalent viscous damping ratio with respect to the rotational speed of the brake discs and with respect to the disc stiffness (top) and friction coefficient (bottom)

The upper figure shows the equivalent viscous damping ratio for a change in the brake disc stiffness over the rotation speed. An increased stiffness for the disc thus results in a higher risk of squeal noise. The increase at lower speeds is bigger than at higher speeds. The lower figure shows the variation of the friction coefficient in addition to the speed change. It can be seen a positive effect of the increase of the friction coefficient in the low speed range and a negative effect in the higher speed range. Highlighted are the speeds without sensitivity to the friction coefficient. The next step

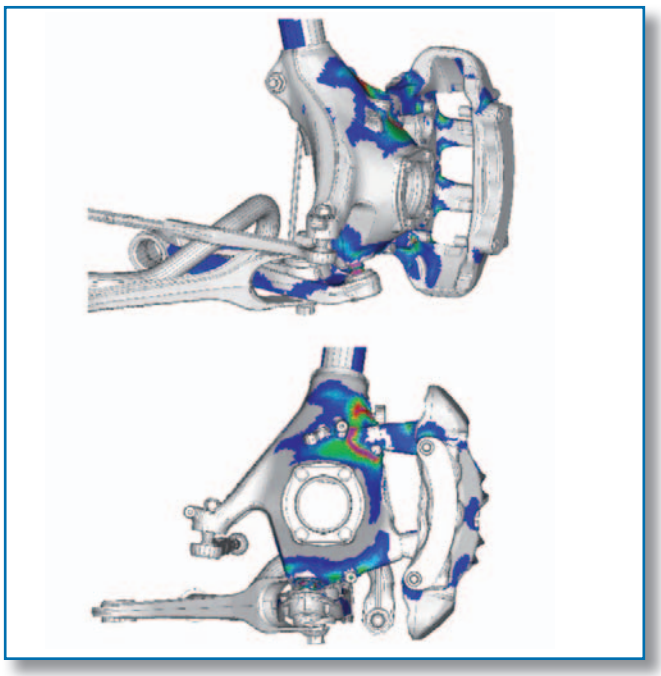

Figure 6: Real Mode 73, areas with high strain energies

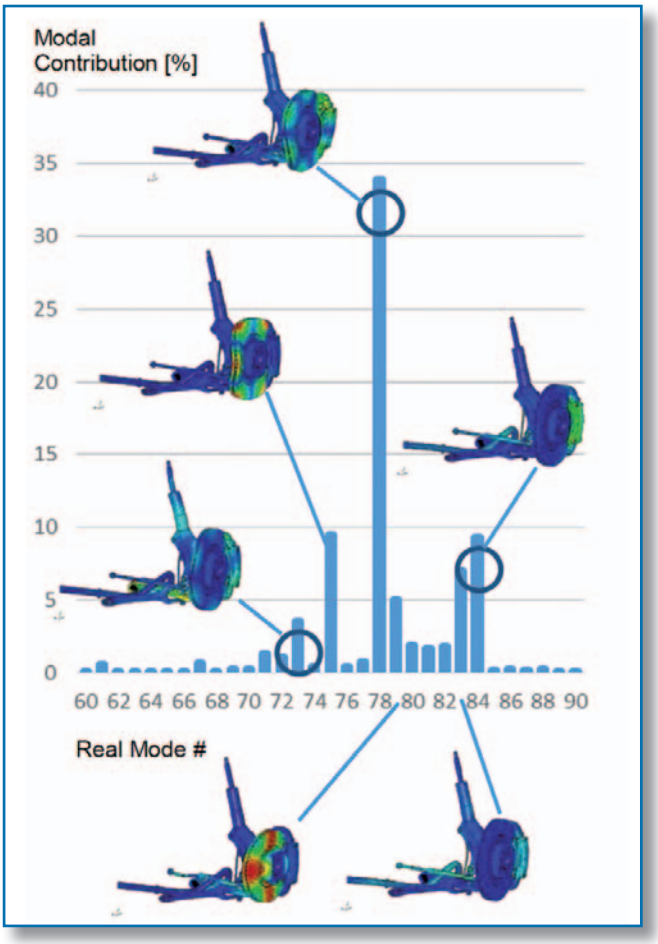

Figure 5: Participation of the real modes in the complex mode at 1700 Hz in percent

to understand the system behaviour better is provided by the participation of the real modes in a potentially unstable complex mode (Fig. 5).
Real mode 78 dominates the influence of real modes on complex mode at 1700 Hz with a participation factor of almost 35%. Real mode 75 and 79 show deformations mainly in the brake disc, while modes 83 and 84 show a deformation of the caliper. In contrast to the other modes with high participation, real mode 73 shows an influence of many components of the system.

A more detailed analysis of the real modes is using the strain energy distribution. Figs. 6, 7 and 8 shows the strain energy of mode 73, 78 and 84 in two different viewings. The brake disc and hub are hidden, so the components behind become visible. High strain energies are in the range of the knuckle and the brake caliper.

5. Step 2: Sampling for Detailed Investigation

A further step in understanding the system behaviour, a second sampling is performed based on the results of the first analysis step. The second objective of this step is to quantify the potential for improvement by simulation.

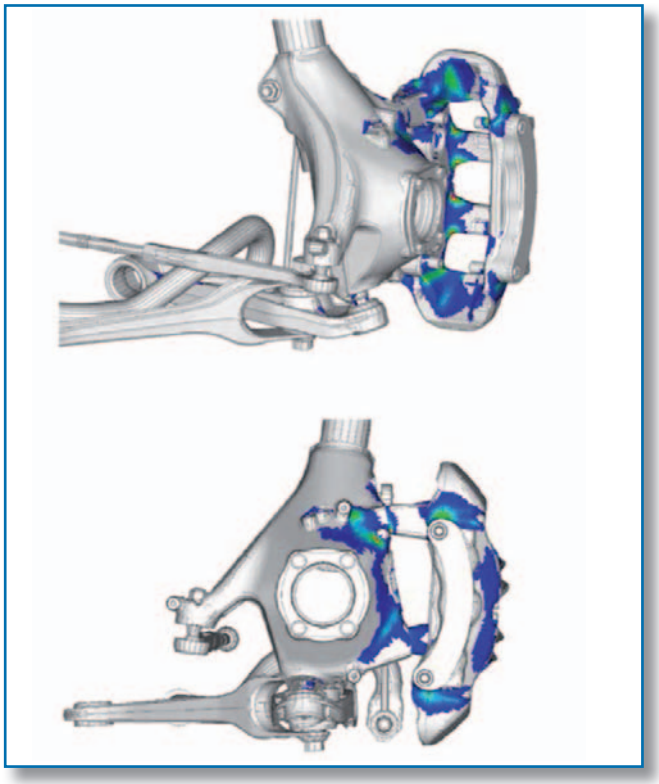

Figure 7: Real Mode 78, areas with high strain energies

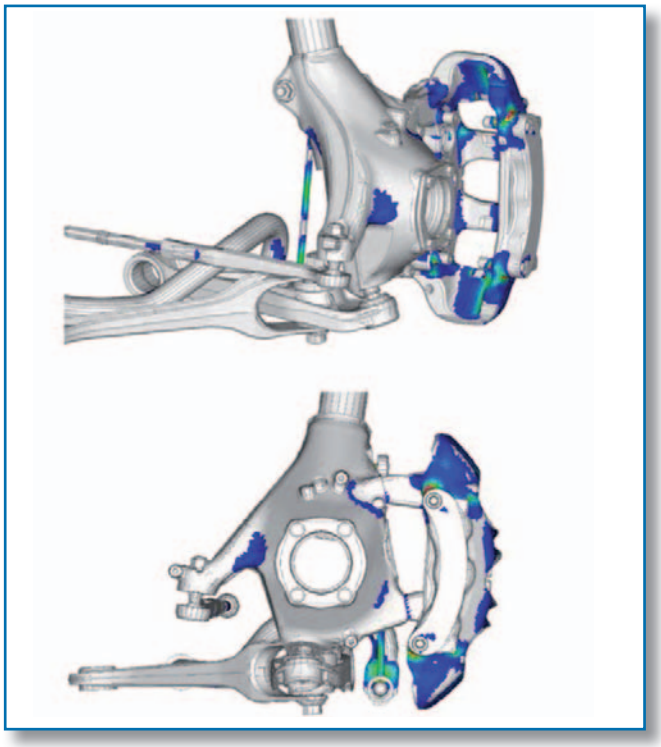

Figure 8: Real Mode 84, areas with high strain energies

The focus here is, as an example, the stiffness of the components, which have high strain energy in important real modes. In this case, these components are the knuckle and the brake caliper. Both are sampled with five different stiffness values. In addition, many rotation speeds are used, as this is possible in PERMAS [3] without significant impact on the computation time.

Fig. 9 shows that the system behaviour is more stable at a higher stiffness of the two components. The influence of the caliper is much stronger than that of the knuckle. This sampling method can be also applied to other components.

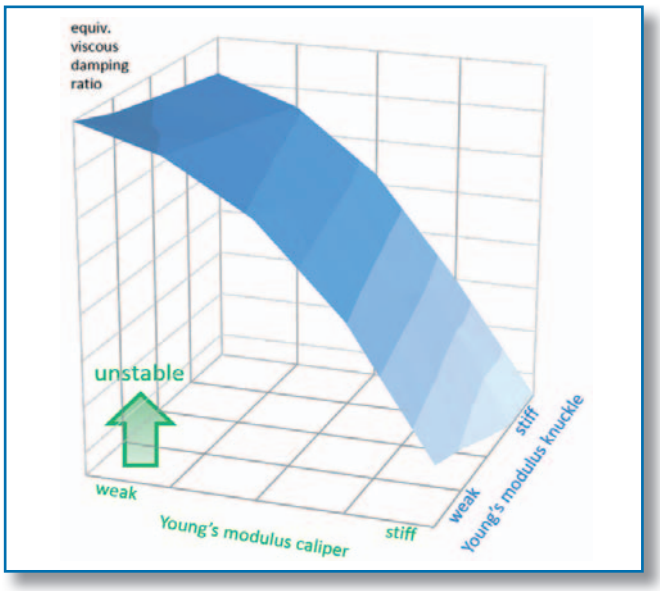

Figure 9: Effect of component stiffness on the equivalent viscous damping ratio

6. Summary and Conclusions

Parameters such as the brake pressure, the rotational speed of the brake, the friction coefficient between the brake disc and brake pad, and the elastic modulus of the brake disc can be varied in PERMAS by sampling in a single simulation run and therefore fast and efficient. The resulting stability map expands significantly the knowledge about the expected NVH performance and the robustness of the brake system for a variety of parameter combinations. In addition, the sampling, as shown by the example, is very useful for further steps of detailed analysis. Due to the very efficient new approaches, the runtimes for PERMAS sampling (about 5 hours for 7,110 samples) are significantly shorter than classical methods for parameter variation. The additional information on the stability map supports the development of a robust low-noise braking system.

www.intes.de

7. References

[1] Carvajal Gonzalez, S.: "Application of PERMAS in virtual brake development", Finite Elements in Engineering Applications, Proceedings of the 11th PERMAS User's Conference, Heidelberg, Germany, 2012, ISBN 978-3-926494-12-2

[2] Ast, M., Kirchgäßner, B.: "Brake Squeal Analysis with PERMAS", Finite Elements in Engineering Applications, Proceedings of the 9th PERMAS User's Conference, Stuttgart, Germany, 2008, ISBN 3-926494-08-5

[3] PERMAS Version 15: "PERMAS User's Reference Manual", INTES Publications No. 450, Stuttgart, Germany 2014

Simulation of Hyperelastic Sealings

C. Gebhardt and N. Nagl
CADFEM GmbH, Grafing bei München, Germany

Summary
Sealings are mission critical components in many industrial applications. Compared to the price of complete systems, where they are used, sealings are relatively inexpensive. However, the Failure of sealings very often ends in significant consequences. Sealings are essential and complex subsystems and their design requires deepened knowledge of materials, loading conditions and failure mechanisms. Today, simulation technologies allow to compute the behavior of sealings with the occurring effects like material nonlinearity, contact and fluid pressure penetration in an parametric, persistent workflow. As a leading software product for this kind of physical questions, ANSYS Mechanical software is widely used to get knowledge in the design of sealings and understanding how to improve them for a functional and reliable behavior. Starting from material data from test specimen, stress strain curves can be imported into ANSYS, which are used to describe the material by traditional material models like Mooney Rivlin, Ogden and Yeoh, or newer formulations like the response function model. Robust contact technology speed up simulation and engineering time and ensure an accurate behavior of the simulation model. Especially for sealings, the area of fluid pressure for 2D and 3D applications can be computed in conjunction with the contact area automatically, which leads to less engineering effort by preventing manual estimation and iterating contact and pressure modelling. Because of the parametric and persistent approach of ANSYS, from CAD, to meshing, material, boundary conditions and solution, a lot of variations can be computed in a short period of time. Beside of a better understanding, this helps engineers to work on changes, which have the best effect and results in the best performance. The influence of uncertainties can also be evaluated, so that the engineer can see the product performance outside of perfect world conditions for a robust and reliable sealing behavior.

KEYWORDS
Hyperelastic material, sealing, fluid pressure penetration, ANSYS, nonlinear material, Neo-Hookean, Mooney Rivlin, Ogden, response function

1: Introduction
The interaction of sliding parts and hyperelastic sealings is a decisive criterion for reliability and functionality in designing hydraulic systems. In case of component failure the entire system may fail. An example for this statement is the Challenger mission in 1986, in which a faulty O-ring was the cause of the accident. A prediction of the tightness and thus a functional dependability is top priority in designing of sealing component. Using finite element simulation tools, such as ANSYS, a broad knowledge can be obtained before producing prototypes that facilitates the interpretation of seals and systems, ensuring the functionality.

In ANSYS Mechanical components with hyperelastic material behavior can be simulated. For this purpose state of the art material models are available inside the simulation environment representing the hyperelasticity.

2: Problem description
Sealings are used in many applications. In this paper a hydraulic piston system is examined for tightness. A piston is sealed by a sealing package consisting of a hyperelastic o-ring and a sealing made of plastics material. Fluid pressure acts on the piston, which propagates along the gap between piston and cylinder, until it encounters the sealing package. The result is a deformation of the sealing package due to the pressure load. Following the pressure propagation the piston is displaced in radial direction. This load step for example represents a tilting of an extended piston. The goal is to ensure the tightness and persistent functionality of the hydraulic piston system after tilting.

3: Modeling
The 3D FEM calculation of the hydraulic system is performed by a static structural analysis. The hydraulic system consists of a

- piston (structural steel),
- cylinder (structural steel),
- sliding rings (PTFE),
- sealing ring (PTFE) and an
- O-ring (hyperelastic elastomer).

The individual components are shown in figure 1. It shows the 3-D symmetry model which was

used for calculating the load scenarios.

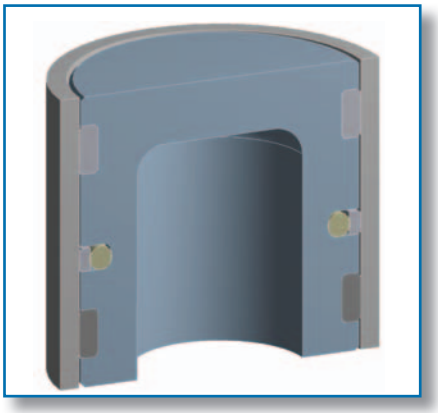

Figure 1: 3D view of the hydraulic sealing system model including piston, cylinder, slide rings, o-ring and sealing ring

For a symmetric behavior of the model the symmetry faces are defined as frictionless support. In addition, the piston is fixed by a fixed support resulting in zero displacement for DOFs ux, uy and uz. The boundary conditions are shown in figure 2.

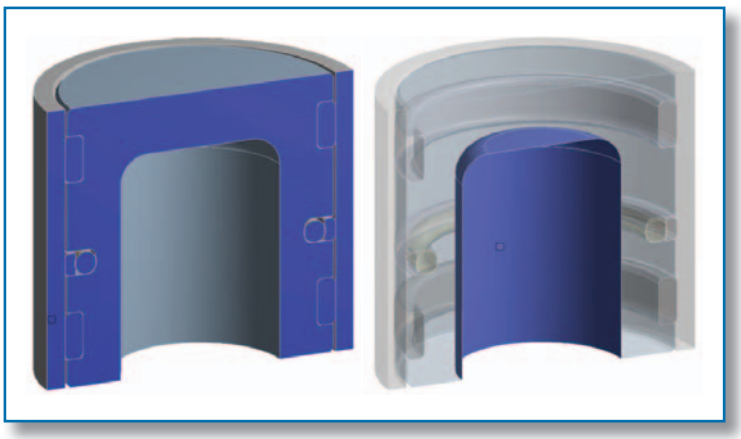

Figure 2: Left: blue colored surfaces represent the frictionless support; right: blue colored surfaces show the fixed support definition

The simulation is divided in 3 load steps.

- 1st load step: assembling
- 2nd load step: fluid pressure of 100 bar
- 3rd load step: radial displacement of 0.3 mm

In the first load step, the individual components are assembled leading already to a deformation of the elastic O-ring. The reason is the geometric penetration between the O-ring and the seal or piston, which is shown in figure 3.

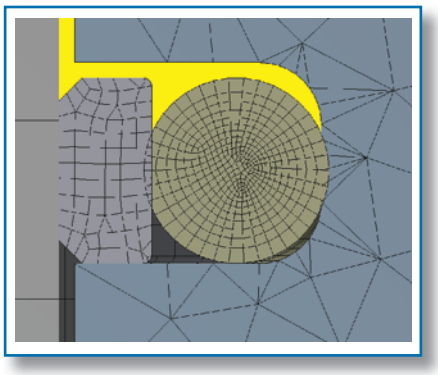

Figure 3: Detailed view of the mesh; geometric penetration between o-ring and sealing ring or piston; yellow colored: fluid

In the second load step, a fluid pressure of 100 bars is applied on top of the piston, which propagates along the free gap to the sealing package which deforms due to the loading. In Figure 3, the fluid is shown schematically in yellow color.

The last load step represents the tilting of the piston. At the beginning the gap between piston and cylinder is 0.5 mm. In this load step the cylinder is loaded with a displacement of 0.3 mm in radial direction which leads to a side load of 153 kN so that the gap at the one side decreases and at the opposite side increases. Furthermore, the sealing package and the slide rings are loaded or unloaded depending on the position. The displacement of the cylinder is applied to the outer surface which can be seen in Figure 4.

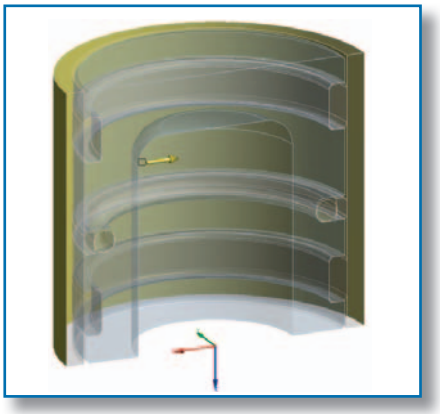

Figure 4: Yellow colored: outer cylinder surface loaded with a displacement

4: Hyperelastic Material Modeling

a. Hyperelasticity

Hyperelasticity is a material nonlinearity in structural mechanics which describes the behavior of highly elastic material such as rubber or a certain variety of plastics. The occurring deformation of hyperelastic materials is usually as large that resulting strains of 100 % and more appear. The relationship between the stress and strain is nonlinear. In general, hyperelastic materials do not show a linear elastic behavior, like known for low loaded structural steel. The stress-strain curve for a linear material (for example, steel in the elastic range) and a hyperelastic material is shown in figure 5.

Hyperelastic materials have an incompressible, elastic material behavior, which means that the deformed component adapts its origin shape after unloading. For describing the hyperelastic behavior several types of loading are necessary to determine correct material parameter. Therefore, uniaxial tension and compression testing as well as biaxial tensile and shear testing is required. The complex material behavior is derived via the strain-energy density, which is often expressed as a polynomial.

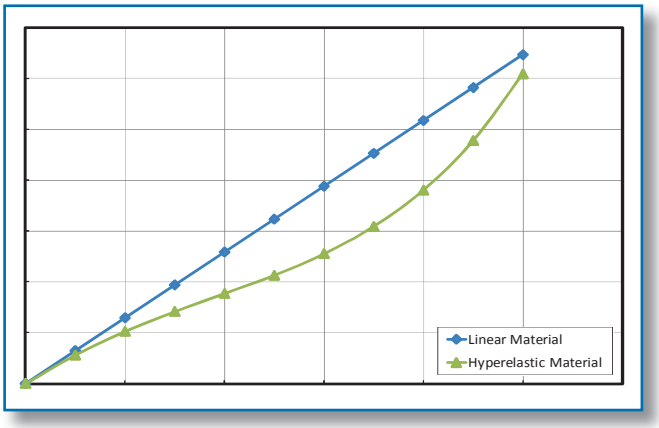

Figure 5: Linear and hyperelastic material behavior

Model	Applied Strain Range [2]
Neo-Hookean	Up to 30 %
Mooney-Rivlin	< 100 % (2nd + 3rd order) < 200 % (5th + 9th order)
Ogden	Up to 700 %
Yeoh	< 300 %
Polynomial	< 300 %

b. Material models with isotropic hyperelastic behavior

In 3D FEM simulation the hyperelastic material behavior is simulated by using material models. To describe these materials an approach for the strain energy W is made which depends on the invariants I_1, I_2 und I_3 [2].

$$W = W(I_1, I_2, I_3) \quad (1)$$

Those three invariants are defined by the elongation λ which is

$$\lambda = \frac{L}{L_0} = \frac{L_0 + \Delta u}{L_0} = 1 + \varepsilon_E \,. \quad (2)$$

In equation (2) ε_E represents the engineering stress.

$$I_1 = \lambda_1^{\,2} + \lambda_2^{\,2} + \lambda_3^{\,2} \quad (3)$$

$$I_2 = \lambda_1^{\,2}\lambda_2^{\,2} + \lambda_2^{\,2}\lambda_3^{\,2} + \lambda_3^{\,2}\lambda_1^{\,2}$$

$$I_3 = \lambda_1^{\,2}\lambda_2^{\,2}\lambda_3^{\,2}$$

The corresponding stress is the derivative of the strain energy function with respect to strain component [1]:

$$S_{ij} = \frac{\partial W}{\partial E_{ij}} \equiv 2\frac{\partial W}{\partial C_{ij}} \quad (4)$$

with

S_{ij} = components of the second Piola-Kirchhoff stress tesor
W = strain-energy function per unit undeformed volume
E_{ij} = components of the Lagrangian strain tensor
C_{ij} = components of the right Cauchy Green deformation tensor, representing invariants I_1, I_2 und I_3

The strain energy function W is approximated by a mathematical material model. Nowadays the user has a large variety of materials available which are based upon the polynomial formulation

$$W = \sum_{i+j=1}^{n} c_{ij}(\overline{I_1} - 3)^i(\overline{I_2} - 3)^j + \quad (5)$$

These include Neo-Hookean, Mooney Rivlin, Ogden or Yeoh. If there are experimental data of the hyperelastic material available, the material models can be fitted onto the data to determine the corresponding coefficients which are necessary to describe the behavior. Apart from this another formulation can be used, the so-called Response Function method, where material's stress-strain-curves of test specimen are used directly instead of an approximation by polynomial formulations.

The simplest hyperelastic material model is Neo-Hookean which consists of only two parameters and the formulation can be derived by setting n = 1, $c_{01} = 0$ and $c_{10} = \mu/2$.

$$W = \frac{\mu}{2}(\overline{I_1} - 3) + \frac{1}{d}(J-1)^2 \quad (6)$$

The strain should not exceed 30 % in the uniaxial case. The following table provides an overview of the strain range for each hyperelastic material models.

Another material model is represented by the Mooney-Rivlin family. There are 2-, 3-, 5- or 9-term Mooney-Rivlin material models. The more terms describe the material behavior, the better higher strains can be described. The two term Mooney-Rivlin model can be obtained by the polynomial formulation for n = 1 which leads to

$$W = c_{10}(\overline{I_1} - 3) + c_{01}(\overline{I_2} - 3) + \frac{1}{d}(J-1)^2. \quad (7)$$

A material model which is suitable for strains up to 700 % is Ogden. The strain-energy function W for the Ogden model is

$$W = \sum_{i=1}^{n}\frac{\mu_i}{\alpha_i}\left(\overline{\lambda_1}^{\alpha_i} + \overline{\lambda_2}^{\alpha_i} + \overline{\lambda_3}^{\alpha_i} - 3\right) + \sum_{i=1}^{n}\frac{1}{d_i}(J-1)^{2i} \quad (8)$$

with the parameter α_i.

ANSYS offers the possibility of curve fitting to determine parameters for the hyperelastic material models. Hyperelastic curve fitting is a tool to obtain material constants for the model based on experimental data.

For the Neo-Hookean and Mooney Rivlin material model a linear fitting and for Ogden a nonlinear fitting is executed. In case of nonlinear fitting initial parameters are necessary.

The hydraulic system includes a hyperelastic component therefore the material behavior has to be defined. Experimental data to describe the hyperelasticity can be used. A material model is selected and a fitting is performed. Figures 3 to 7 show the data points and the fitted curves created with the respective material model for a uniaxial, biaxial and shear material behavior. Figure 3 shows a fitting with the simplest material model Neo-Hookean. It can be seen that in the range up to strains of 0.3 the material behavior can be approximated acceptable. This model is not suitable for larger strains.

Comparing the curves with the Mooney-Rivlin formulation (figures 4 to 6), we see that the fitting gets better with an increasing number of terms. A high accuracy can be obtained with the 5-term Mooney-Rivlin model. In figure 7, the nonlinear fitting is shown with the Ogden model. Comparing the 5-term Mooney-Rivlin fitting with the Ogden fitting, we can see that there is no difference between both models.

For the simulation of the hydraulic system, the hyperelastic behavior of the O ring is simulated using the 5-term Mooney-Rivlin material model, as the fitted curves suit to the experimental data. An exception to the usual material models is the response function method. The "model" is based on the approximate determination of the derivatives of the strain energy function for the invariants I_1 and I_2. The stress for hyperelastic, incompressible materials is given by [1]

$$\sigma_{ij} = -p\delta_{ij} + dev\left[2\frac{\partial W}{\partial I_1}b_{ij} - 2I_3\frac{\partial W}{\partial I_2}b_{ij}^{-1}\right] \quad (9)$$

δ_{ij} = Kronecker delta (δ_{ij} = 1, i = j; δ_{ij} = 0, i ≠ j)
p = pressure
b_{ij} = left Cauchy-Green deformation tensor

The volumetric deformation is defined as

$$p = \frac{\partial W}{\partial J}. \quad (10)$$

If the derivatives W_{I1}, W_{I2} and W_J are known or can be determined from experimental data, the stresses can be calculated. The deviatoric stress is determined by the deformation $W_j = \frac{\partial W}{\partial J}$ and the derivatives of the elastic potential function $W_{I1} = \frac{\partial W}{\partial I_1}$ and $W_{I2} = \frac{\partial W}{\partial I_2}$. These derivatives are called response functions. For isotropic hyperelasticity they can be achieved analytically. However, they can also be obtained from experimental data fitting the parameter of the potential functions onto the experimental data.

According to the equations [1]

$$\sigma_{11} = 2\left(\lambda_1^{\,2} - \lambda_1^{\,-1}\right)\left[\frac{\partial W}{\partial I_1} + \lambda_1^{\,-1}\frac{\partial W}{\partial I_2}\right] \quad (11)$$

for uniaxial tension,

$$\sigma_{11} = 2\left(\lambda_1^{\,2} - \lambda_1^{\,-4}\right)\left[\frac{\partial W}{\partial I_1} + \lambda_1^{\,2}\frac{\partial W}{\partial I_2}\right] \quad (12)$$

for equibiaxial tension and

$$\sigma_{11} = 2\left(\lambda_1^{\,2} - \lambda_1^{\,-2}\right)\left[\frac{\partial W}{\partial I_1} + \frac{\partial W}{\partial I_2}\right] \quad (13)$$

for pure shear, there is a correlation between the stress, deformation and response functions. The experimental data include information on the measured deformation and stress. The only unknown is the equation for the response functions. We get the volumetric response function from equation (10) either analytically or from experimental

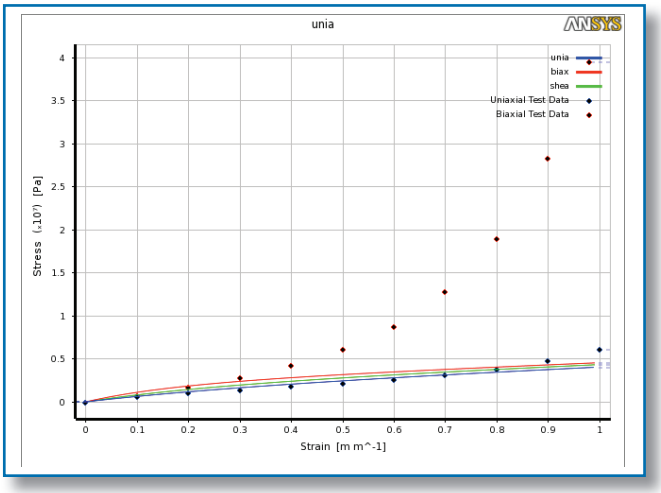

Figure 6: Neo-Hookean fitting

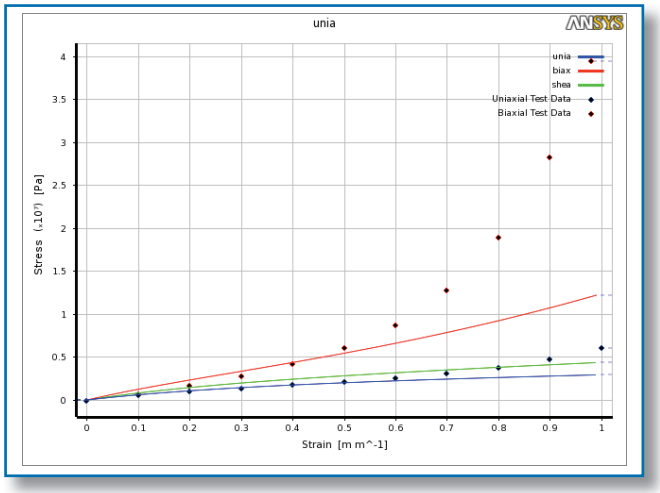

Figure 7: Mooney-Rivlin 2nd order fitting

data from volume ratio against pressure. From the experimental data, the pressure can be determined, which leads to the volumetric response function. Thus, all parameters are available so that the stress can be calculated.

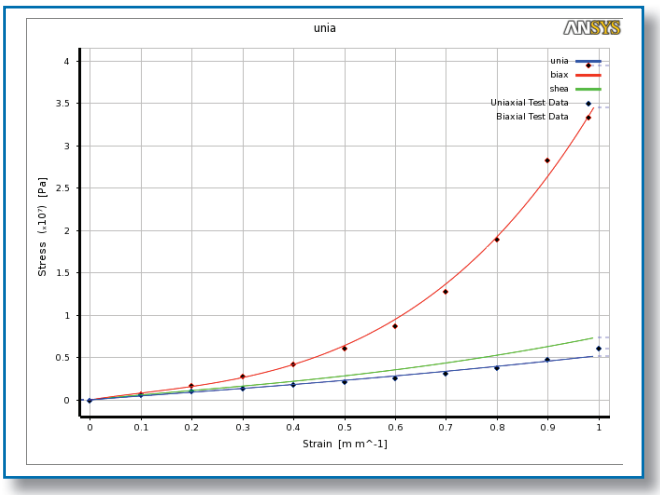

Figure 8: Mooney–Rivlin 3rd order fitting

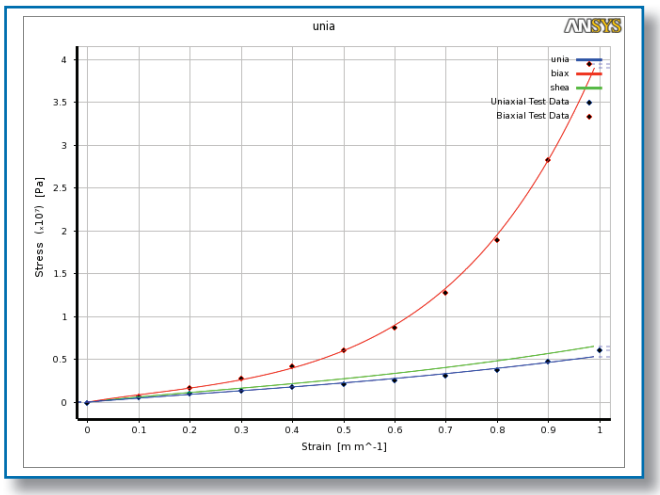

Figure 9: Mooney–Rivlin 5th order fitting

5: Simulation Technology Fluid Pressure Penetration [1]

Pressure-penetration loads can si-mulate surrounding fluid or air penetrating into the contact interface, based on the contact status.

In this simulation a fluid pressure of 100 bars is applied onto the cylinder. Pressure penetration simulates the fluid propagating from top of the piston to the sealing package. The fluid pressure penetrates into the contact interface from predefined locations depending on the actual contact situation.

The propagation of the fluid pressure starts from defined locations, e. g. surfaces. The starting points are displayed red in figure 11. In these areas the contact status is checked. Depending on the contact pressure and the deformed shape, the fluid pressure propagation continues and finds an equilibrium in several numerical iterations.

Compared to a manual definition of the fluid pressure areas, a key advantage of this technology is that the area where pressure is acting does not have to be defined prior to calculation. The contact status with the corresponding contact pressure is detected and the propagation of the fluid pressure is calculated automatically. If the contact status between the O-ring, sealing the piston and the cylinder changes, the fluid pressure acting area with the corresponding surfaces is adjusted automatically. For example, the O-ring is deformed by the acting fluid pressure which leads to changes in the contact status of several contacts. The contact status switches from “open” to “close” resulting in a new pressure acting surface. This has effects on the applied fluid pressure. Thus, an iterative procedure to determine the surface is necessary which happens automatically when using fluid pressure penetration.

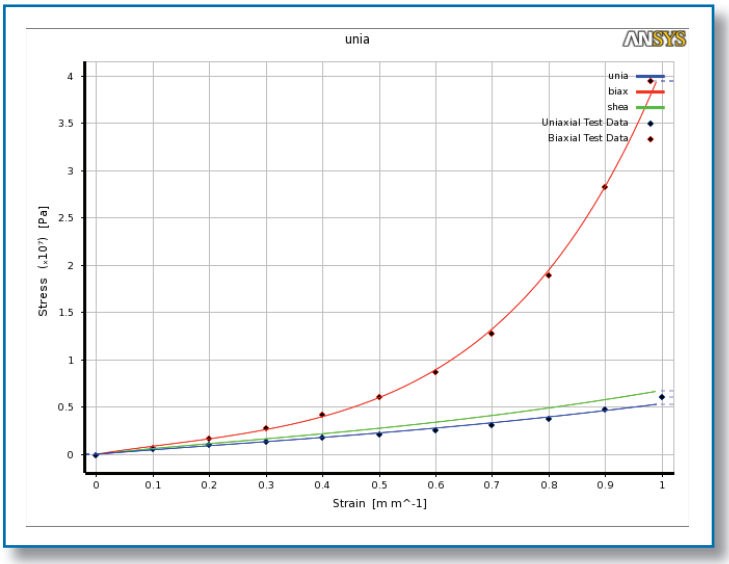

Figure 10: Ogden 3rd order fitting

6: Results

a. 1st Load step – Assembly

In the first load step, all components of the hydraulic system are assembled, i.e., the geometric penetration caused by the O-ring is pushed back, to describe the assembling situation. In figure 12 the sealing package and the sliding rings are displayed. Figure 13 shows a detailed view of the sealing package. The O-ring has been compressed and limits together with the sealing ring the fluid acting area.

After the assembly the maximum occurring strains of hyperelastic o-rings are 11 per cent and are distributed evenly around the circumference (see figure 12).

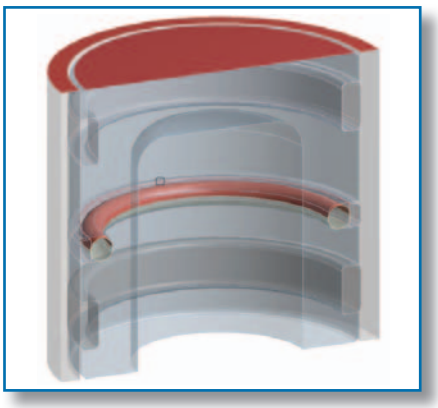

Figure 11: Red colored: defined surfaces for starting fluid pressure

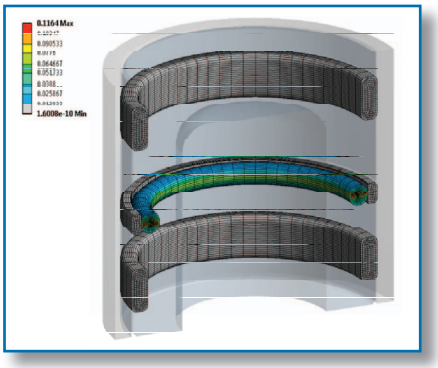

Figure 12: Global view of the strain distribution of the hyperelastic sealing after the 1st load step (assembling)

b. 2nd Load step – Fluid Pressure Loading

In the second load step a fluid pressure of 100 bars is applied.

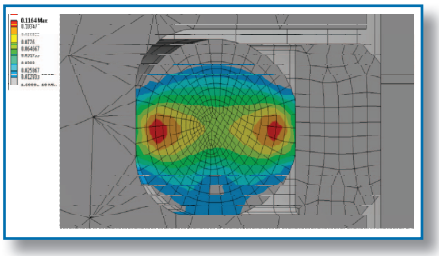

Figure 13: Detailled view of the strain distribution of the hyperelastic sealing after the 1st load step (assembling)

The fluid pressure propagates from the predefined starting points (see section 5) depending on the current contact situation und compresses the hyperelastic O-ring even more. The O-ring fits into the groove of the piston and pushes the sealing ring towards the piston wall. Figure 14 shows a detailed view of the O-ring and the sealing ring. The maximum strains of the O ring are 41 per cent.

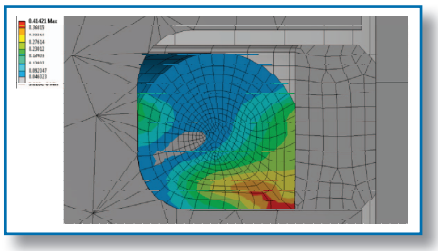

Figure 14: Strain distribution of the hyperelastic sealing after the 2nd load step (fluid pressure acting)

c. 3rd Load step – Radial Displacement

In the last load step, the cylinder is displaced radially by 0.3 mm, which is simulates a tilting of the piston in the extended position. Due to the one-sided load the pressure distribution between the the components changes so that one side is loaded higher than the opposite one. Figure 15 shows the distribution of the contact pressure between the sealing ring and the piston.

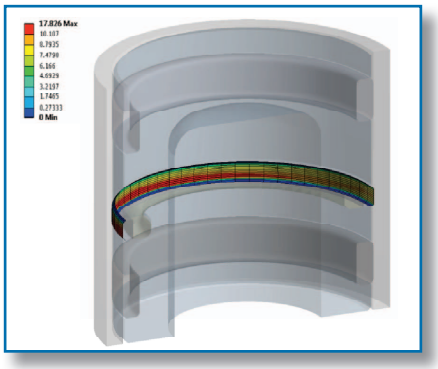

Figure 15: Contact pressure between the sealing ring and piston after the 3rd load step (radial displacement)

A result of the one-sided loading is that the strains of the O-ring rise compared to the load step 2. In figure 16 and 17 we can see the strain distribution of the O-ring.

The maximum strains are 47 per cent. In figure 18 the fluid pressure of the contact elements is displayed. The applied pressure of 100 bars has been propagated until the sealing pakkage. The functionality of the hydraulic system can be ensured, as the combination of O-ring and sealing completely seals the system. A propagation of the pressure and a resulting pressure drop can be avoided.

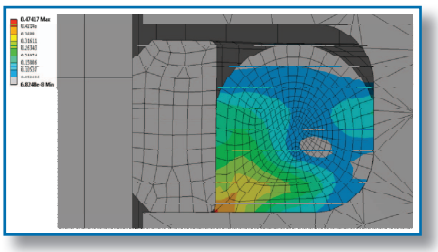

Figure 16: View: left side of the model; Strain distribution of the hyperelastic sealing after the 3rd load step (radial displacement); The resulting gap between piston and cylinder has decreased to 0.2 mm.

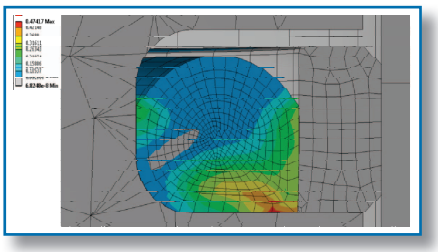

Figure 17: View: right side of the model; Strain distribution of the hyperelastic sealing after the 3rd load step (radial displacement); The resulting gap between piston and cylinder has increased to 0.8 mm.

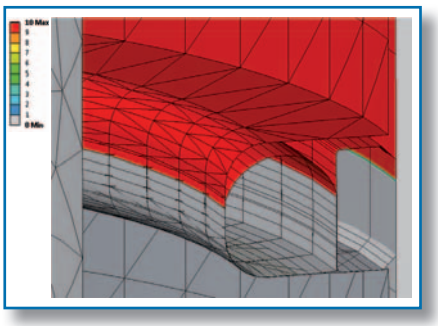

Figure 18: Fluid pressure of the contact elements in MPa;

7: Conclusion

The design and evaluation of sealings under load is a challenging engineering task. Beside of sophisticated material behavior, complex contact situations, assembling processes and loading

situations have to be accounted for. Especially, the pressure load and the resulting pressure applied surfaces and changing contact areas require powerful technology to support the engineer to set the focus on the design process. In the previous case, the simulation has shown the reliability of the hydraulic system, as the piston is sealed with the sealing package against the cylinder and the tightness remains during the side load.

For the design of seals, the 3D FEM simulation turns out to be a useful tool. Following to a preliminary design, a systematic variation of design parameters can be done for a better understanding of the whole design space. Using the optimization software optiSLang the sensitivities of the individual input parameters are calculated and powerful statistics visualization help to improve the design. The ANSYS software thus offers a comprehensive and innovative 3D FEM solution for the calculation of reliable and robust hyperelastic sealings.

www.cadfem.de

References

[1] ANSYS, Inc., 2013. ANSYS 14.5 Help. Manual

[2] CADFEM GmbH, 2013. Berechnung von Gummi- und Schaumstoffbauteilen. Seminar material

State of the Art in Failure Prediction in Crashworthiness

A. Haufe[1], F. Andrade[1], M. Feucht[2] and F. Neukamm[2]
[1]DYNAmore GmbH, Stuttgart, Germany, [2]Daimler AG, Sindelfingen, Germany

Abstract

In recent years, the requirements on passive safety of cars have grown to high standards, leading to a permanent demand on an increase in simulation accuracy. Additionally, demands on fuel efficiency and CO_2 – reduction are confronting car body desig–ners with the need of substantial weight reduction. Hence, the increasing use of high and ultra-high strength steel grades for bodies in white is a major trend. At the same time, simulation techniques are urged to predict formability and crashworthiness performance of sheet metal designs much more accurately than in the past in a continuous attempt to reduce the number of expensive physical tests and to simultaneously accelerate the development process.

This contribution focuses on the link between sheet metal forming and crashworthiness simulation for high strength steel grades. Transferring the forming simulation results to other simulation disciplines like crashworthiness will eventually give more insight into the effects of pre-straining and possible pre-damaging emerging from production processes on the target discipline. From an industrial point of view, the whole topic has gained a lot of attention, especially because the crashworthiness performance of bodies in white is assessed typically by finite element simulations. Therefore maintaining and enhancing predictability of the applied models is of great importance. The present contribution is meant to give an introductory overview on this topic.

Introduction

As a consequence of the worldwide tendency in reducing CO_2 emissions by producing lighter and more energy-efficient products, the demand for accurate predictions regarding material behavior and eventually failure has greatly increased in recent years. In particular in the automotive industry, reliable strategies for effectively closing the gap between forming and crash analysis are sought, since different forming operations (i.e. production steps) may strongly affect the crashworthiness of the produced parts. In this scenario, a correct description of the mechanical degradation and fracture of the used sheet material seems indispensable. In order to link the two simulation disciplines 'sheet metal forming' and 'crashworthiness', one has to study the numerical approaches that are used in both fields. In both disciplines, finite element shell formulations still are the state-of-the-art discretization with a typical element size in the range of 0.2 mm (sheet metal forming) up to 3 mm (crashworthiness). In this scenario, the most important difference when transferring results from one discipline to the other is the constitutive model.

As usual, the constitutive behavior is described with the help of history variables whose evolution is given by internal equations. Experimental methods like tension test, tension-compression tests or biaxial tests of sheet metal are then carried out to identify the necessary macroscopic material parameters for the applied plasticity model. However, the choice of the constitutive model very often depends on the discipline in question. For instance, anisotropic strain rate independent elasto-plasticity is generally preferred in the case of forming analysis, mainly due to their high accuracy in describing local plastic straining. On the other hand, isotropic strain rate dependent elasto-plastic models, whose numerical algorithms provide extreme short computation time, are commonplace in the industry when undertaking crashworthiness simulations. As a matter of fact, the use of different constitutive models in both disciplines poses a real challenge when mapping history data from the forming onto the crash model.

Concerning the improvements achieved in crashworthiness analysis, great effort has been done throughout the past years regarding the treatment of crack formation and propagation. Currently, state-of-the-art is the use of failure models that accumulate damage on an incremental basis. Most incremental models are based on the observations made by Bridgman [4], who found that the failure strain in metallic materials depends on the hydrostatic pressure. Examples of constitutive models commonly used are the Gurson model with the extensions by Tvergaard and Needleman [13] and the failure model of Johnson and Cook [7]. A common disadvantage in crash models adopted by the industry nowadays is the fact that the sheet metal parts used in crashworthiness computations are usually assumed to be as in a virgin-like material delivery state.

This disregards the changes in constitutive properties resulting from previous treatments in the process chain of the sheet metal part manufacturing, including deep-drawing processes. In the easiest case, a local increase of the yield stress caused by work hardening can be expected. Since plastic pre-straining also results in a reduction of the remaining strain to failure, the effect of pre-damaging must be taken into account, preferably in a phenomenological manner. This, in turn, leads to the conclusion that not only plastic strains, but also the damage occurred during forming simulations should be taken into account. The models discussed in the following were implemented in a collaboration of Daimler AG and DYNAmore GmbH and are available in the simulation suite LS-DYNA [9].

Constitutive modeling in sheet metal forming

In sheet metal forming, anisotropic elasto-plasticity models applied to classical 5-parameter shell elements are predominantly used, while limiting states (i.e. the instability of the sheet in a physical sense) are usually investigated by post-processing schemes through the use of the so-called forming limit curves (FLC) as the one depicted in Fig. 1. Essentially, this method

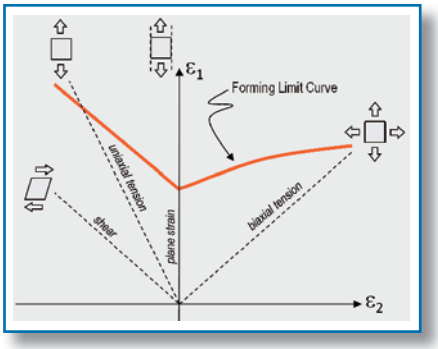

Figure 1: Classical forming limit curve

compares principal strains on the sheet plane with an experimentally measured forming limit curve to check whether a part will have necks and cracks during the forming process. One example of a widely adopted constitutive model in the industry is the one proposed by Barlat, Lege and Brem [3]. These authors have defined an anisotropic yield function for the plane stress case which can be written as (1)

$$\Phi = a|K_1 + K_2|^M + a|K_1 - K_2|^M + c|2K_2|^M = 2\sigma_Y^M$$

where (2)

$$K_1 = \frac{\sigma_x + h\sigma_y}{2} \quad and \quad K_2 = \sqrt{\left(\frac{\sigma_x - h\sigma_y}{2}\right)^2 + p^2\tau_{xy}^2}$$

In the equations above, σ_γ is the actual yield stress; a, c, h and p are anisotropy parameters usually calculated from planar Lankford parameters. Furthermore, the mo-del is based on the assumption of isochoric plastic behavior, thus, by definition, plastic yielding leads to a volumetric plastic strain rate $\dot{\varepsilon}_p^{pl}$ equal to zero. Normally, but not always, the effects of strain rate are neglected in forming analysis, simplifying the use of the underlying plasticity model.

Constitutive modeling in crashworthiness applications

As already mentioned in this paper, the constitutive modeling in crashworthiness has to fulfil different requirements as in forming simulations. Perhaps, the most crucial requirement is the computational solution time of a given load case, especially in the case of large, full car crash models. Features that are important in the process simulation are therefore intentionally omitted in crash simulations. In practice, this requires different models for the different disciplines, although it basically involves exactly the same materials and the same geometries. Among several simplifications undertaken in crash models, anisotropic plasticity, commonly adopted in forming simulations, is substituted by classical, isotropic von Mises plasticity with strain rate dependence, i.e., (3)

$$\Phi_{vM} = \sqrt{3J_2} - \sigma_{vM}(\bar{\varepsilon}^{pl}, \dot{\bar{\varepsilon}}^{pl}) = 0$$

Usually, hardening curves for several strain rates are numerically calibrated to match experimental data and are introduced into the finite element code through tabulated curves. This approach is simpler and more pragmatic than the use of analytical extrapolation functions for the hardening curves, but has proved reasonably effective for industrial purposes.
Nevertheless, if one aims to predict fracture of the sheet metal in crashworthiness analysis, a damage and failure has to be considered. The effects of pre-straining and pre-damaging that take place in the forming process have to be taken into account in the crash simulation in order to get an accurate prediction of sheet failure. A proper mapping procedure from the forming to the crash discretization is necessary also. Such a mapping scheme poses unfortunately a quite difficult task since it involves operation on different mesh refinements. Usually, finite element meshes in forming analysis are much finer than the ones used in crash models. Furthermore, the plastic strains obtained in the forming simulation cannot be directly transferred onto the crash mesh. Spurious mesh dependence, which occurs under special conditions like local softening and strain localization, unfortunately complicates a consistent mapping between the dissimilar meshes in a direct manner. Obviously, this poses a further challenge when linking both disciplines as the plastic strains have to be somehow adjusted from the forming to the crash model to properly compensate for the mesh dependence effect (Neukamm et al. [12]).

A generalized scalar damage model for forming and crashworthiness simulations

A straightforward approach to in-corporate damage and failure in plasticity models is the application of a scalar damage model in the classical form:

$$\sigma^* = \sigma_{nom}(1-\tilde{D}) \tag{4}$$

While the simplicity of such models might be striking, if the modification of the stress components by D is regarded only, one typically overlooks the many and complex evolution equations for the scalar variable D. Variations of such models, taking linear or nonlinear damage accumulation or path dependency into account, the consideration of orthotropic properties or the characteristic of the applied stress state, element size dependency and much more have been published. Furthermore, typically element erosion (i.e. deletion of single elements from the computation database) must be regarded as the daily engineering approach in crashworthiness studies. Clearly, this needs further contemplation in order to erode an element only if a minimum number of integration points (per element) still contribute to the load carrying capacity.

In the following, the damage and failure model GISSMO (Generalized Incremental Stress-State dependent damage MOdel), which has demonstrated to be a very a successful approach to unify some of the many available plasticity-based models, will be presented. The main properties of the implementation are a combination of the proven features of failure description provided by damage models for crashworthiness calculations, together with an incremental formulation for the description of material instability and localization. For crashworthiness simulations of ductile materials, the correct description of instability and localization also influences the predictive accuracy of computational results. In general, it cannot be assumed that the stress states experienced by the material will be the same in a forming process compared to a subsequent crash loading scenario. Hence, the model includes not only the description of failure (Bai & Wierzbicki [2]), but also the functionality to provide an incremental, path-dependent treatment of instability. This is necessary in order to avoid the most obvious limitation of the traditional FLC which considers only the final state of deformation at the end of a forming process, and therefore does not take into account possible changes in the strain path (Müschenborn & Sonne [11]). In order to allow for the treatment of arbitrary strain paths in the prediction of localization and failure, incremental formulations were chosen. The concept is to independently accumulate a measure for forming intensity F,

$$\Delta F = \frac{n_F}{\varepsilon_f(\eta)} F^{\left(1-1/n_F\right)} \Delta\varepsilon_v \tag{5}$$

and a measure for damage D,

$$\Delta D = \frac{n_D}{\varepsilon_f(\eta,\xi)} D^{\left(1-1/n_D\right)} \Delta\varepsilon_v \tag{6}$$

Here, the parameters η and ξ are stress triaxiality- and Lode-parameters, respectively defined as:

$$\eta = \frac{I_1}{3\sqrt{3J_2}} \quad \text{and} \quad \xi = \frac{3\sqrt{3}}{2}\frac{J_3}{J_2^{\frac{3}{2}}}, \tag{7}$$

where I_1, J_2 and J_3 are the invariants of the stress tensor and stress deviator. Eq. (6) represents a generalization of the well-known linear accumulation rule for damage as proposed by Johnson & Cook and follows in its basic concept the ideas of Mackenzie et al. [10]. The parameters $n_D = n_F$ define the nonlinear accumulation of the instability or damage measure. This in turn allows calibration of the model to data obtained from multi-stage coupon tests. The current equivalent plastic strain increment is denoted by $\Delta\varepsilon_v$. The quantity ε_f represents the triaxiality- and Lode-parameter dependent failure strain, which is used as a weighting function in this relation. Input of the failure strain is done through a tabulated curve definition of failure strain values vs. triaxiality (and vs. Lode-parameter if needed in a 3D discretization).

As soon as the forming intensity measure F reaches unity, coupling of accumulated damage to the stress tensor using the effective stress concept proposed by Lemaitre [8] is initiated. When curve data of triaxiality-dependent material instability for shell discretizations are used, this value represents the onset of instability in sheet metal and therefore the limit of mesh-size convergence of the results. For a practical application of the model in finite element computations with rather coarse element sizes, this corresponds to the beginning of the need for regularization for different mesh sizes. The basic idea is to regularize the amount of energy that is dissipated in the process of crack development and propagation and follows the ideas presented by de Borst et al. [5]. This results in a variation of the rate of stress reduction through element fading and is achieved by modifying Lemaitre's effective stress concept:

$$\sigma^* = \sigma\left(1-\left(\frac{D-D_{crit}}{1-D_{crit}}\right)^m\right) \quad for \quad D \geq D_{crit} \tag{8}$$

This introduces an exponent m which governs the rate of fading of the stress and may be defined

depending on the current element size. Equation (8) is in fact a generalization of Lemaitre's classical principle of effective stress where Lemaitre's formulation can be promptly recovered if one sets $m = 1$ and $D_{crit} = 0$.

When damage reaches unity, fracture is assumed to have taken place and the integration point is no longer able to bear any external loading. An equation like (8) seems to be necessary for a more accurate description of fracture for non-proportional strain paths, that is, when the triaxiality or the Lode angle is not constant throughout the deformation process.

Non-proportionality is a key issue in the prediction of localization, instability and failure. In fact, FLD-based approaches, which are very popular in sheet forming analysis and proved quite effective in many practical applications for mild steels, have been struggling for years to find a suitable method for high strength steels. On the other hand, damage accumulation like the one defined in Eq. (6) is a rather simple and elegant way to deal with the problem. Although many issues regarding the damage accumulation still remain open, Eq. (6) can provide results that are very satisfactory in practical applications.

Finally and well understood, spurious mesh dependence is a common issue in finite element analysis. Especially in the case of ductile fracture prediction, this aspect plays a major role. Briefly speaking, different mesh sizes will lead to different strains in the simulation results if strain localization arises. The issue of spurious mesh dependence has been subject of research since the 1980's and many solutions have been proposed in the literature. Among them, the non-local method, formulated either through integral or gradient-dependent strategies, seems to provide an effective solution to this issue. However, in order to be effective, these methods require very fine mesh sizes that are smaller than the physical length scale of the cracking or process zone of the material. For steel alloys, this would be typically $l_e < 0.5mm$ which is – at present – prohibitive in forming and crash analysis.

Another way of dealing with spurious mesh dependence is by compensating its effects. In this respect, GISSMO allows the user to define element size-dependent factors which adjust the fracture curve to the corresponding element size. However, it is important to mention that this strategy does not solve the problem of spurious mesh dependence, but rather artificially compensates its effects in the calculation of damage. As a matter of fact, it seems that currently there is no other known method for large element sizes. Nevertheless, practical experience by the authors has shown that this method is generally quite useful in crash analysis.

Path-dependent accumulation for the instability criterion

We now focus attention on the treatment of material instability or localized deformation to be applied in the GISSMO model.

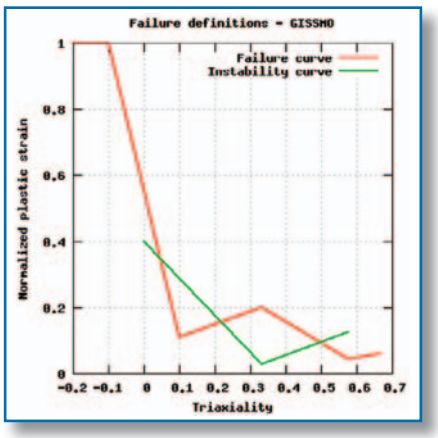

Figure 2: GISSMO calibrated curves for damage/failure (normalized and idealized).

The basic idea is to determine the strains at the onset of localization from tests under constant stress state (proportional loading). For example, tensile tests with various notch radii, shear tests and biaxial tests can be used to determine such strains for different stress states. The resulting forming limit curve is then used as an input for the instability model. Furthermore the curve may be used as weighting function for the path-dependent accumulation of necking intensity, F, up to the expected point of instability. In general, the localization behavior of material definitions in numerical simulation depends on the yield locus and evolution of the yield stress. Since a direct determination of yield curves from specimen tests for the post-critical range of deformation is not possible, stress extrapolation based on engineering assumptions (or models) is used. Due to this approach, the parameters used in the extrapolation procedure characterize the material behavior also in the post-critical range and consequently define the onset of mesh-dependency. For this reason, a damage-based regularization for the post-critical range is adopted in GISSMO.

The implementation in the GISSMO model uses the transformed FLC curve in coordinates of equivalent plastic strain and triaxiality as a weighting function for the accumulation of "Forming Intensity", which, in this context, is actually a measure of the remaining formability. For this purpose, the forming limit curve may be converted into the linear incremental formulation that was originally proposed by Johnson & Cook:

$$\Delta F = \frac{\Delta \varepsilon_v}{\varepsilon_{v,loc}} \qquad (9)$$

Here, $\varepsilon_{v,loc}$ is the equivalent plastic strain at the onset of insta-

bility, defined as a function of triaxiality η. In this case, F is accumulated linearly, while the function of equivalent plastic strain to necking represents a triaxiality-dependent weighting function. When F reaches unity, necking is expected to occur. Proportional loading is included as a special case and leads to identical results as given by the standard FLC.

Recent publications indicate a possible nonlinearity in the relation of damage and equivalent plastic strain, even for proportional strain paths. Weck et al. [14] performed measurements on a material that showed a rather exponential relation between strain and damage in form of void growth. It seems a reasonable assumption that the development of plastic strain up to necking also obeys a nonlinear relation, yet no method that would allow for a direct measurement of this quantity is known to the authors.

Nevertheless, a nonlinear accumulation is incorporated in the GISSMO model (Eq. 5) using the same relation as for the accumulation of ductile damage to failure (Eq. 6). An identification of parameters for this relation will hardly be possible from direct physical measurements, but rather by means of reverse engineering simulations of multi-stage forming processes.

Numerical calibration of a dual-phase steel

In this section, the calibration of a dual-phase steel using GISSMO is presented. The experimental results of six different specimens have been used in the calibration procedure: two uniaxial tensile, two shear, one notched tensile and one biaxial test (Fig. 3). A more detailed description of model calibration is found in Effelsberg et al. [6]; while a comparison to other popular approaches is discussion in Andrade et al [1]. Ideally, each test would deliver a stress path with constant triaxiality so that the fracture curve could be directly measured from the experiments. However, in reality, the strain path and, consequently, the triaxiality are not constant in most specimen geometries. This strongly suggests that the calibration of GISSMO has to be carried out numerically by adopting a reverse engineering strategy in order to identify the fracture curve. Furthermore, aspects like element formulation and plasticity model also influence the final calibration. In the present contribution, we will adopt state-of-the-art fully integrated shell elements and a von Mises elasto-plastic model. These choices are based on definitions that are very often used in car crash simulation. Notwithstanding their importance, the effects of the strain rate on the failure behavior have been disregarded in this paper and will be subject of further investigation in a future contribution.

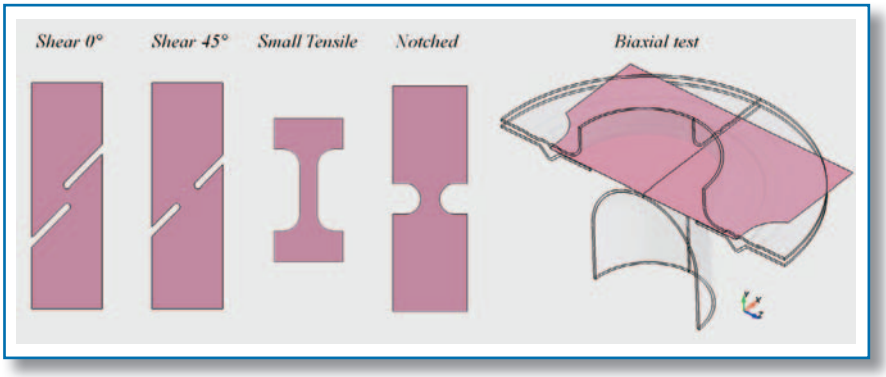

Figure 3: shear 0°, shear 45°, small tensile, notched tensile and biaxial specimens

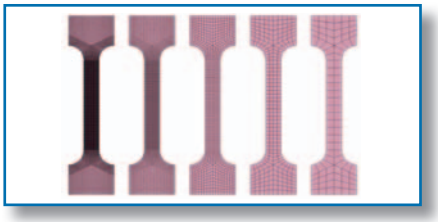

Figure 4: Large tensile specinnen with different mesh sizes: 0.5, 1.0, 2.5, 5.0 and 10.0 mm

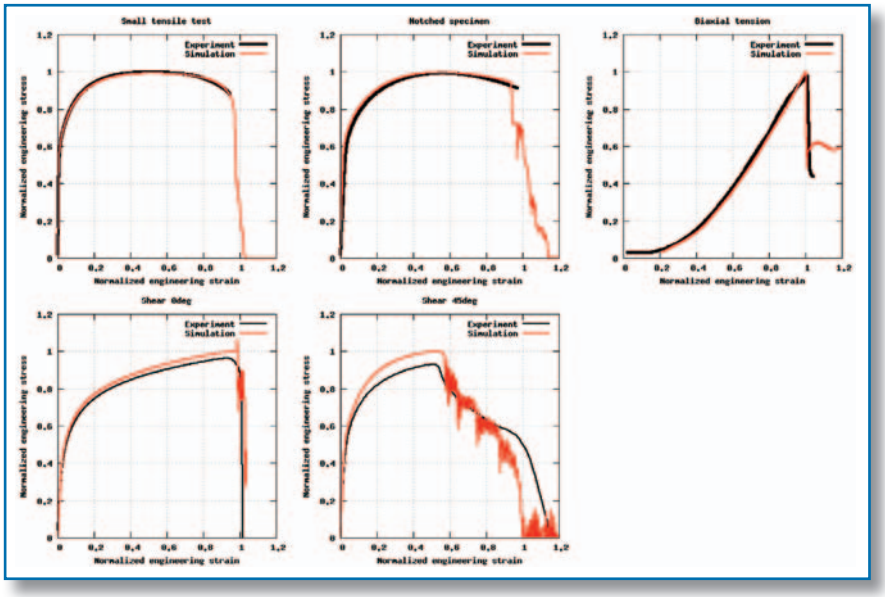

Figure 5: Simulation results with GISSMO – comparison with experimental data.

The element size used in the discretization of the specimens was 0.5mm, which is in fact relatively small. In real car crash simulations, the element size is much larger, nowadays ranging from 1.5 mm up to 5.0 mm. For the calibration of mesh dependence, a large tensile specimen was used considering different mesh sizes as shown in Fig. 4.

Fig. 5 shows the calibrated curves using a damage exponent n = 2.0 and a fading exponent m = 2.5. Notice that the definition of the fading exponent is only meaningful if the instability feature of the model is used.

Concerning the sensitivity to spurious mesh dependence, the simulation of a large tensile specimen is typically carried out with the calibrated curves of 0.5mm. Based on this computation, the element size dependent regularizing factors, that scale the fracture curve in order to get a similar failure pattern upon mesh refinement, are numerically calibrated. Fig. 6

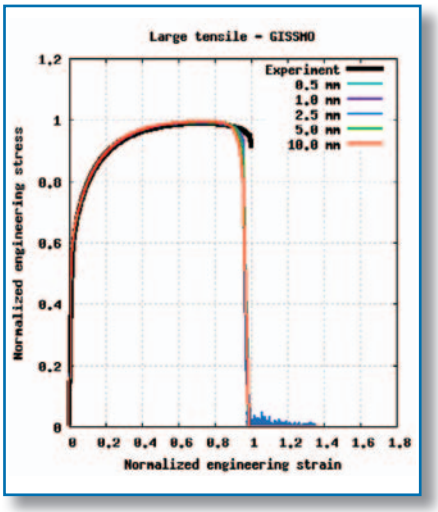

Figure 6: Regularisation of large tensile specimen with different mesh sizes.

shows the results for 5 different meshes: 0.5 mm, 1.0 mm, 2.5 mm, 5.0 mm and 10 mm. It becomes evident that, for this particular tensile specimen, GISSMO provides a near perfect match for all element sizes. One should keep in mind though that, beyond spurious mesh dependence, the inherent inaccuracy arising from coarse geometrical discretization is also present in the case of larger elements. Thus, the regularizing factors of GISSMO inevitably end up correcting both effects. Unfortunately, it is very difficult to say how much is due to spurious mesh dependence and how much due to coarseness of geometrical discretization.

B-pillar under dynamic side crash

As alluded before, the choice of the constitutive model in the simulation is based on many criteria, including also the solution time necessary for a single simulation run. In an industrial environment, several simulations with different configurations and load cases have to be undertaken on a frequent basis in order to properly assess a given product within practicable time. The automotive safety requirements of side impact load cases are quite challenging due to the severity of the dynamic loadings under real-world conditions. Therefore, there is a clear tendency of employing high strength (dual-phase and complex-phase steels) and ultra-high strength (boron steel) steel grades in the design of B-pillars. These components play a crucial role in minimizing intrusion by external agents and thus significantly reducing the severity of injuries suffered by the vehicle's occupants. In such drastic scenario, it is quite important to determine whether the B-pillar is able to resist the external loadings without major cracks. To this end, plenty of simulations are carried out where modifications in the material type, geometry, position and number of spot welds, among others, are performed.

In this section, we present the results of the simulation of a B-pillar subjected to an impact orthogonal to the component in question. Typically present B-pillars consist of different steel alloys that simultaneously maximize ductility and minimize occupant injury. In the present case, these were carefully calibrated individually using the GISSMO model in conjunction with von Mises plasticity. The element size adopted (L_e = 3.0 mm) is compatible to mesh refinements used in full car crash simulations. Figure 7 shows a comparison of the simulation result with the experiment. As can be seen, the simulation could reproduce the experimental results with great accuracy, where the critical area of that particular design was very effectively identified. The conduction of the experiment corresponding to the simulated configuration has allowed a further validation of the methodology employ-

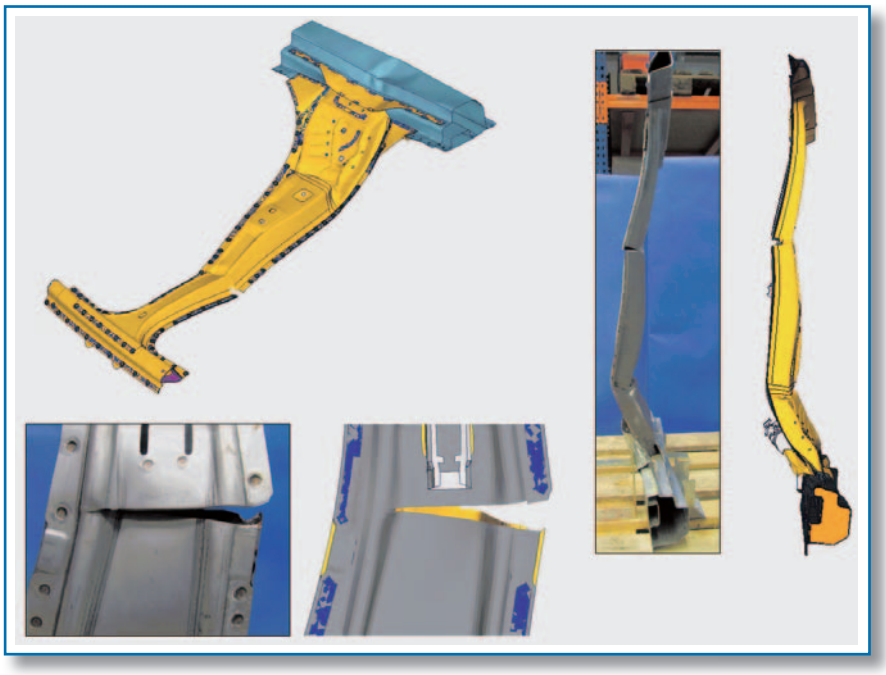

Figure 7: Comparison between simulation and experimental results of the B-pillar

ed for the prediction of fracture of high strength and ultra-high strength steels. This kind of validation is a crucial step in the development chain so that the project engineers can rely on the adopted constitutive models and numerical modeling techniques to properly assess newer designs. Finally, the computational solution time of the present simulation was around 45 minutes running on 96 processors. Such low solution time is only possible if one disregards unimportant details and concentrates efforts in proper numerical modeling strategies where the methodology using GISSMO in conjunction with classical von Mises plasticity has proven quite effective for this application.

Conclusions

Indeed, a more accurate modeling and prediction of fracture are essential for increasingly more efficient designs in the industrial scenario. However, current modeling and computational capabilities impose some limits in the design process. In this respect, GISSMO seems to be a very useful option in order to predict ductile failure considering the effects of pre-strain and pre-damage and still being practicable using the computational resources available today. In this manner, the project engineer is able to better understand the effects of the different processes of the manufacturing chain on the load-carrying capacity of produced parts, resulting in more efficient, reliable and robust designs.

One important point that should be mentioned is that complex scalar damage models seem to lack uniqueness of solution, that is, different calibration strategies may lead to identical results. Nevertheless, the range of possible solutions tends to decrease by increasing the number of experiments upon which the parameter identification is based. Furthermore, the engineer's experience also plays a role in order to get accurate calibration results. This aspect may be seen as a big disadvantage, but it is just a natural consequence of the flexibility that such models provide. Especially in the case of newer and modern metallic alloys, the observed material behavior is often difficult to describe using analytical failure functions that are based on microstructural mechanisms. Therefore, phenomenological approaches like GISSMO are quite convenient for treating practical problems using current technological resources.

www.dynamore.de

References

[1] Andrade, F., Feucht, M., Haufe, A., 2014, *On the prediction of material failure* in LS-DYNA: *A comparison between GISSMO and DIEM,* 13th International LS-DYNA Users Conference, June 8-10, Dearborn, MI, USA.

[2] Bai Y., Wierzbicki T., 2008, *Forming Severity Concept for Predicting Sheet Necking Under Complex Loading Histories,* Int. Journal of Mechanical Sciences 50, pp. 1012-1022.

[3] Barlat, F., Lege, D.J., Brem, J.C., 1995, *A Six-Component Yield Function for Anisotropic Materials,* Int. Journal of Plasticity 7, pp. 693-712, 1991 693-712.

[4] Bridgman, P.W., 1952, *Studies in Large Plastic Flow and Fracture, With Special Emphasis on the Effects of Hydrostatic Pressure,* McGraw Hill Inc., New York.

[5] De Borst R., Sluys LJ, Mühlhaus H.-B., Pamin J., 1993, *Fundamental Issues in Finite Element Analyses of Localization of Deformation.* Engineering Computations 10, pp. 99-121.

[6] Effelsberg, J., Haufe, A., Feucht, M., Neukamm, F., DuBois, P., 2012, *On the Parameter Identification for the GISSMO Damage Model,* 12th International LS-DYNA Users Conference, Detroit.

[7] Johnson, G.R., Cook, W.H., 1985, *Fracture Characteristics of Three Metals Subjected to Various Strains, Strain Rates, Temperatures and Pressures.* Fracture Mechanics, 21, pp. 31-48, 1985 31-48.

[8] Lemaitre J., 1985, *A Continuous Damage Mechanics Model for Ductile Fracture,* Journal of Engineering Materials and Technology 107, pp. 83-89.

[9] Livermore Software Technology Corporation, 2014, LS-DYNA Keyword User's Manual Volume II – Material Models.

[10] Mackenzie, A.C., Hancock, J.W., Brown, D.K., 1977, *On the Influence of State of Stress on Ductile Failure Initiation in High Strength Steels,* Eng. Frac. Mech. 9.

[11] Müschenborn W., Sonne H.-M., 1975, *Influence of the Strain Path on the Forming Limits of Sheet Metal.* Arch. Eisenhüttenwesen 46(9), pp. Eisenhüttenwesen 46 (9), pp. 597-602.

[12] Neukamm, F., Feucht, M., Haufe, A., 2009, *Considering Damage History in Crashworthiness Simulations,* 7th European LS-DYNA Users Conference, Salzburg.

[13] Tvergaard, V., Hutchinson, J.W., 1992, *The relation between crack growth resistance and fracture process parameters in elastic-plastic solids,* J. of the Mech. And Phy. of Solids, 40, pp1377-1397.

[14] Weck A., Wilkinson DS, Toda H., Maire E., 2006, *2D and 3D Visualization of Ductile Fracture,* Advanced Engineering Materials 8 (6), pp. 469-472.

Selected Conference Announcements

For an up-to-date conference schedule, please also visit the new GACM website at www.gacm.de/activities/conferences/

6th GACM Colloquium on Computational Mechanics

(together with 3rd ECCOMAS Young Investigators Conference (YIC) and 3rd Aachen Conference on Computational Engineering Science (AC.CES)).

Location: RWTH Aachen University
Time: July 20 – 24, 2015
Webpage: http://www.yic.rwth-aachen.de/

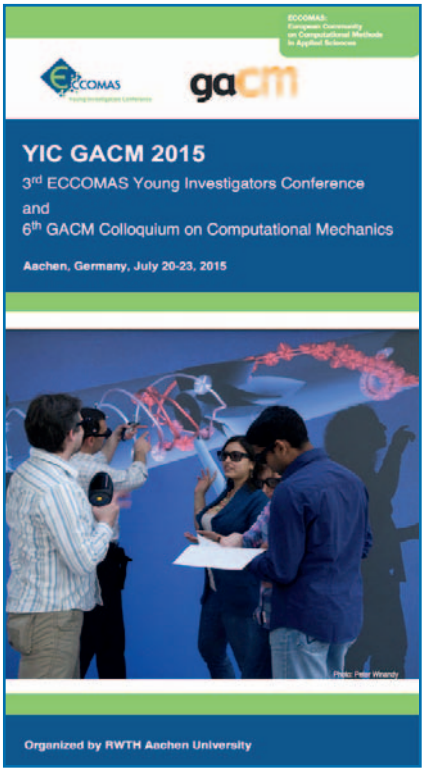

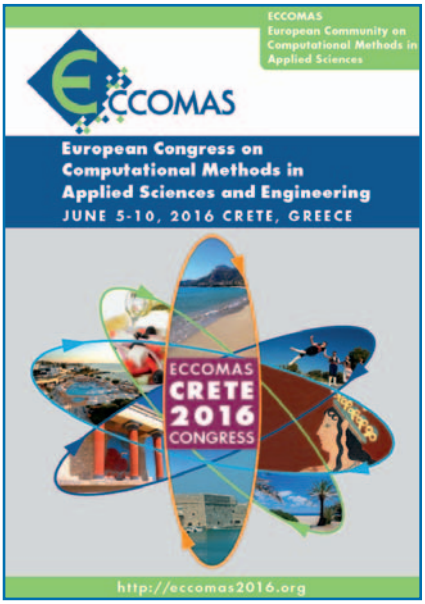

7th European Congress on Computational Methods in Applied Sciences and Engineering

Location: Crete Island, Greece (Creta Maris Conference Centre)
Time: June 5 – 10, 2016
Webpage: http://www.eccomas2016.org/

12th World Congress on Computational Mechanics

(together with 6th Asia-Pacific Congress on Computational Mechanics).

Location: Seoul, Korea (Coex Convention & Exhibition Center)
Time: July 24 – 29, 2016
Webpage: http://www.wccm-apcom2016.org/

ECCOMAS Thematic conferences

25 ECCOMAS Thematic Conferences will be organized in 2015.
A complete list can be found at http://www.eccomas.org/

the german association for
computational mechanics

Institute for Computational Mechanics
Technische Universität München
Boltzmannstrasse 15
D-85747 Garching, Germany
Phone: +49 89 289-15300
Fax: +49 89 289-15301
email: gacm@lnm.mw.tum.de
Internet: www.gacm.de